SURFACE ENHANCED RAMAN SCATTERING SPECTROSCOPY ON SILVER COLLOIDS FOR TRACE ANALYSIS

BY

EDITH LIZETTE TORRES TAPIA

A DISSERTATION PRESENTED TO THE GRADUATE SCHOOL
OF THE UNIVERSITY OF FLORIDA IN
PARTIAL FULFILLMENT OF THE REQUIREMENTS
FOR THE DEGREE OF DOCTOR OF PHILOSOPHY

UNIVERSITY OF FLORIDA

1986

ACKNOWLEDGMENTS

I would like to express my gratitude to Dr. James D. Winefordner for his constant advice and concern throughout my stay at the University of Florida.

I am very grateful to Dr. José Alberto Lanauze for proofreading this dissertation and for drawing all the figures herein. His endless patience and dedication always inspired me to do better as a scientist and as a person. I would also like to thank my colleagues in Dr. Winefordner's research group and Dr. John G. Dorsey and his research group for their friendship during all these years. The good times that we shared will be forever remembered.

Recognition is also due to Dr. Anna Brajter-Toth and her research group for providing the triply-distilled water used throughout this work and to Dr. Ray von Wandruszka for suggesting the possibility of studying PABA. Thanks also must go to Dr. Joseph H. Simmons, Department of Materials Science and Engineering, for the access to and the use of the Raman system from Instruments S.A. in his laboratory facilities at the University of Florida Research and Technology Park.

Finally, I am very thankful to my parents for their constant love and encouragement which always helped me reach my goals. Without them, this work would not have been possible.

TABLE OF CONTENTS

Page

ACKNOWLEDGMENTS....ii

LIST OF TABLES....v

LIST OF FIGURES....vi

ABSTRACT....ix

CHAPTERS

ONE INTRODUCTION....1

TWO THEORETICAL CONSIDERATIONS....4

The Raman Process....4
The Surface Enhanced Raman Effect....8
The Electromagnetic Model....10
The Short Range Mechanism--Adatom Hypothesis....16
SERS on Metal Colloids....19
Metal Colloids....20
Analysis of Results and Theory of SERS on Metal Colloids....22

THREE A SIMPLE DEVICE FOR SERS STUDIES....30

Introduction....30
Theoretical Concepts....31
Resolution and Resolving Power....31
Light Gathering Power....32
Signal to Noise Expressions....33
Experimental Section....35
Instrumentation....35
Procedure....39
A Comparison Between Two Instruments....41

FOUR ANALYTICAL APPLICATIONS OF SERS ON SILVER COLLOIDS....49

Introduction....49
Experimental....50

Results and Discussion.....51
Characterization of Silver Hydrosols.....51
Qualitative Study.....57
Quantitative Study.....85

FIVE CONCLUSIONS AND FUTURE WORK.....95

REFERENCES.....100

BIOGRAPHICAL SKETCH.....104

LIST OF TABLES

Table		Page
1	List of Reagents	40
2	Specifications of the Monochromators Studied	42
3	Comparison of the Results Obtained with the Monochromators Studied	47
4	SERS Results for Uracil	64
5	SERS Results for Uridine and 6-Amino Uracil	69
6	Effect of the Concentration of Silver Hydrosols on the SERS Signal of 0.75 μg/mL Phenytoin	90
7	SERS Limits of Detection and Calibration Sensitivities for PABA and 2-Aminofluorene	93

LIST OF FIGURES

Figure		Page
1	Energy diagram of a molecule showing the origin of the Rayleigh and Raman scattering effects	6
2	Schematic representations of (A) a prolate and an oblate spheroid, and (B) the axes for axial and azimuthal modes of oscillation for a prolate spheroid	12
3	Dependence on the aspect ratio (a/b): (a) of the dielectric function for axially symmetric and azimuthal oscillation modes; and (b) of the plasma energies for silver spheroids	14
4	Comparison of Raman scattering from an isolated molecule with that of a molecule located near a metal surface	17
5	Graphical representations: (a) of the calculated extinction cross-section for silver prolate spheroids in water for various axial ratios; and (b) of the calculated enhancement for a 1010 cm^{-1} Raman band as a function of excitation wavelength for a monolayer of adsorbate on silver prolate spheroids in water for various axial ratios	26
6	Experimental extinction (——) and excitation profiles (---) for the 1014 cm^{-1} band of pyridine on gold hydrosols	28
7	Experimental arrangement for SERS studies	37
8	Scan of the 459 cm^{-1} Raman band of CCl_4: (A) with the Model 1680B from Spex Industry; and (B) with the Jobin-Yvon Model U1000 from Instruments S.A.	44
9	Scan of the 1005 cm^{-1} Raman band of phenytoin made 1 μg/mL in the silver sols	46
10	Absorption profile of silver hydrosols	52

11 Absorption profile of silver hydrosols 30 min after adding phenytoin to a final concentration of 1 μg/mL.....54

12 Absorption profile of silver hydrosols after adding phenytoin to a final concentration of 1 μg/mL, a-f taken successively every 10 min.....56

13 Absorption profile of silver hydrosols after adding phenytoin to a final concentration of 50 μg/mL, with silver hydrosols aged for 24 hr before adding phenytoin....59

14 Molecular structures of pyrimidine derivatives in ribonucleic acid: uracil and uridine; and 6-amino uracil.....60

15 Scattered intensity (1 cm = 130 cts/s) vs. Raman shift ($\Delta\nu$, cm^{-1}) of (a) 500 μg/mL uracil in water; (b) the silver hydrosols showing the continuum background radiation; and (c) 5 μg/mL uracil in silver hydrosols (SERS spectrum).....63

16 Scattered intensity (1 cm = 130 cts/s) vs. Raman shift ($\Delta\nu$, cm^{-1}) of (a) 500 μg/mL uridine in water; (b) the silver hydrosols; and (c) 5 μg/mL uridine in silver hydrosols (SERS spectrum).....68

17 Scattered intensity (1 cm = 130 cts/s) vs. Raman shift ($\Delta\nu$, cm^{-1}) of (a) 500 μg/mL 6-amino uracil in water; (b) the silver hydrosols; and (c) 50 μg/mL 6-amino uracil in silver hydrosols (SERS spectrum).....72

18 Molecular structures of other adsorbates studied.....74

19 Scattered intensity vs. Raman shift of (a) the silver hydrosols (3 cm = 390 cts/s); (b) 80 μg/mL PABA in water (1 cm = 390 cts/s); and (c) SERS spectrum of 50 μg/mL PABA in silver hydrosols (3 cm = 390 cts/s).....76

20 Scattered intensity (1 cm = 130 cts/s) vs. Raman shift of (a) the silver hydrosols; (b) 0.75 μg/mL phenytoin in water; and (c) 0.75 μg/mL phenytoin in silver hydrosols (SERS spectrum).....79

21 Scattered intensity (1 cm = 130 cts/s) vs. Raman shift of (a) 50 μg/mL naphthalene in silver hydrosols; (b) 50 μg/mL naphthol in silver hydrosols; and (c) 50 μg/mL 2-aminonaphthalene in silver hydrosols.....82

22 Scattered intensity vs. Raman shift of (a) the silver hydrosols (3 cm = 390 cts/s); (b) 50 μg/mL fluorene in silver hydrosols (3 cm = 390 cts/s); and (c) 10 μg/mL 2-aminofluorene in silver hydrosols (1 cm = 390 cts/s).....84

23 Logarithmic calibration plot for PABA at the 1359 cm^{-1} Raman band and for 2-aminofluorene at the 1594 cm^{-1} Raman band.....92

24 Proposed HPLC detectors: (a) flow-through design; and (b) solid support design.....97

Abstract of Dissertation Presented to the Graduate School of the University of Florida in Partial Fulfillment of the Requirements for the Degree of Doctor of Philosophy

SURFACE ENHANCED RAMAN SCATTERING SPECTROSCOPY ON SILVER COLLOIDS FOR TRACE ANALYSIS

BY

EDITH LIZETTE TORRES TAPIA

December, 1986

Chairman: James D. Winefordner
Major Department: Chemistry

The development of surface enhanced Raman scattering (SERS) spectroscopy on silver colloids as an analytical technique is discussed. By taking advantage of the enhanced signals observed in this newly developed technique, the use and performance of a simple and inexpensive device for Raman studies are evaluated. The results demonstrate that SERS on silver colloids can be successfully used for the qualitative determination of N-containing drugs such as p-aminobenzoic acid (PABA), phenytoin, uracil and uracil derivatives as well as N-containing polynuclear aromatic hydrocarbons such as 2-aminofluorene.

Analytical calibration curves of PABA and 2-aminofluorene yield straight lines with the slopes of their log-log plots close to unity. The absolute limits of detection for these compounds were 35 ng and 7 ng, respectively. The reasons for the rather poor

correlation between signal and concentration for the other adsorbates studied are discussed. For some compounds, SERS has the high identification power inherent in all vibrational techniques, with the added advantage of being as sensitive as most luminescence techniques presently used for trace analytical purposes.

CHAPTER ONE
INTRODUCTION

One of the features of Raman spectroscopy that has always been very appealing to researchers is its capability to provide information on the molecular structure of the samples under study. Being a vibrational technique, it complements infrared (IR) spectroscopy but has, in addition, several advantages over it. First, spectral measurements in Raman spectroscopy can be made within the ultraviolet (UV)-visible range. This permits the use of glass or quartz optics and cells, UV-visible sources, monochromators and detectors simplifying in this way the instrumentation needed. Secondly, the entire spectrum can be examined with one instrument, unlike IR spectroscopy which requires several gratings to cover the entire spectral range of interest. A third advantage is that aqueous solutions offer no problem, simplifying in this way sample-handling techniques, especially for the studies of biological systems, inorganic substances and water pollution problems.

The main disadvantage of Raman spectroscopy has always been its poor sensitivity and, although the intensity of a Raman line is linearly related to the concentration of the species excited, precision instrumentation is required to isolate Raman bands which are much weaker than the incident radiation. Therefore, in a normal Raman spectrum, a severe signal to noise ratio problem exists giving poor

results especially for samples which are not optically homogeneous or which fluoresce at the excitation wavelength employed. Resonance Raman spectroscopy involves excitation into a vibronic level of the electronic excited state in order to greatly enhance the Raman cross-sections, in some cases by factors of two to six orders of magnitude. However, under some circumstances, this technique is plagued with fluorescence background from the analyte and concomitant impurities in the sample.

Two of the more sensitive molecular spectroscopic techniques available to the analytical chemist are fluorescence and phosphorescence. Although detection limits down in the picogram level can be obtained with these techniques, not all compounds fluoresce or phosphoresce under normal analytical conditions. This limits their applicability mostly to aromatic analytes. Even then, fluorescence and phosphorescence spectra tend to be structureless due to their broad absorption bands. Furthermore, most aromatic hydrocarbons absorb in the same spectral region, so that selective excitation of one component in a mixture can be difficult. Therefore, the analytical chemist is lacking a simple technique that can combine both the selectivity inherent in a vibrational spectroscopic technique such as Raman spectroscopy and the sensitivity of a luminescence technique.

With the advent of surface enhanced Raman scattering (SERS) spectroscopy, this situation is rapidly changing. This technique consists of observing the regular Raman process at or near metallic surfaces which are properly roughened, detecting in this way Raman bands which can be amplified by factors ranging from three to six

orders of magnitude. Its sensitivity, therefore, is similar to that of luminescence techniques with the added advantage of spectral selectivity. In fact, when the species under study absorbs at the laser frequency used, the resonance enhancement effects and the surface enhancement effects are multiplicative in these systems leading to enhancements as great as ten orders of magnitude. In this case, the metal surface can also lead to additional nonradiative decay channels which will decrease the fluorescence background problem usually encountered in resonance Raman spectroscopy.

Since the SERS technique selectively enhances only certain vibrational modes of the molecule, the spectra tend to be simpler than a normal Raman scattering spectrum. Also, interfering Raman bands from traces of impurities are generally of negligible intensity which simplifies sample-handling and interpretation of the spectra.

The purpose of this study was two-fold: first, to evaluate the use and performance of a simple and inexpensive device for Raman studies which could significantly increase the applicability of the SERS technique; secondly, to perform SERS measurements with this system on molecules of current interest, such as drugs and polynuclear aromatic hydrocarbons, and develop the technique as an analytical method for the measurement of small amounts or concentrations of analytes.

CHAPTER TWO
THEORETICAL CONSIDERATIONS

The Raman Process

Light incident upon a molecule can interact with it by either absorption or scattering. The most frequently used absorption techniques are ultraviolet (UV) absorption spectroscopy, visible absorption spectroscopy and infrared (IR) absorption spectroscopy. In UV and visible absorption spectroscopies, the molecule absorbs a photon (UV or visible light) and is excited to a higher electronic energy level; while in IR, absorption of a photon (IR light) results in excitation of the molecule to a higher vibrational or rotational energy level.

Scattering refers to light deflected at all angles from the direction of incident-light propagation. The interaction of the electric vector of an electromagnetic wave with the electrons of a molecule results in the scattering of the incident light. Such interactions induce periodic vibrations in the electrons of the molecule causing a temporary polarization. As a consequence, the energy of the radiation is momentarily retained in a so-called virtual state, i.e., the incident radiation does not raise the molecule to any particular quantized energy level. After approximately 10^{-15}-10^{-14} seconds, the polarized molecule ceases to oscillate and returns to its original ground level as shown in Figure 1. In doing so, it releases

Figure 1 Energy diagram of a molecule showing the origin of the Rayleigh and Raman scattering effects.

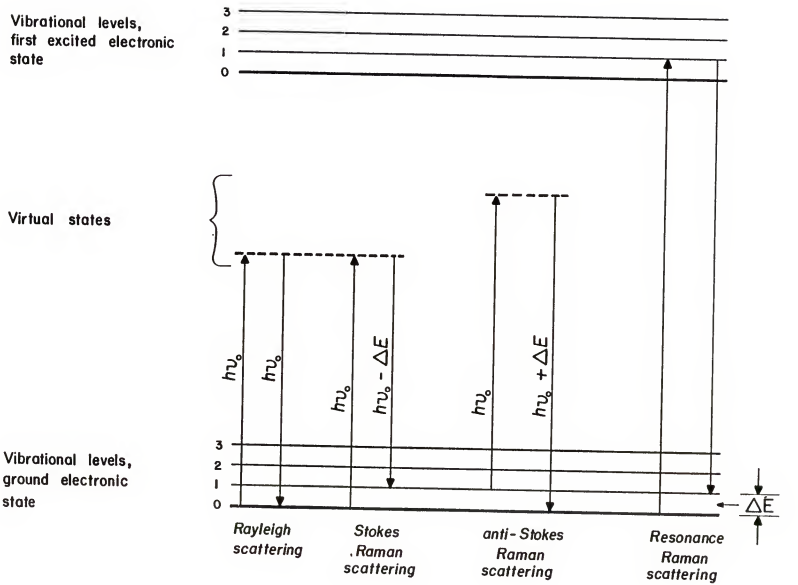
Vibrational levels, first excited electronic state
Virtual states
Vibrational levels, ground electronic state
3
2
1
0
hυ₀
hυ₀
hυ₀ - ΔE
hυ₀
hυ₀ + ΔE
ΔE
Rayleigh scattering
Stokes Raman scattering
anti-Stokes Raman scattering
Resonance Raman scattering

radiation in all directions of exactly the same energy as the source (Rayleigh scattering). However, a small fraction of the excited molecules (10^{-6} or less) may undergo a change in polarizability during one of the normal vibrational modes. This will result in the return of the molecule from the virtual state to the first excited vibrational level of the ground state. The frequency emitted in this transition will be less by a quantized amount that corresponds to the difference in energy between the ground state and the first vibrational level, ΔE, and accounts for the Stokes lines that appear in a Raman spectrum. The incident light may also induce downward vibrational changes which will give rise to anti-Stokes lines, but they will be of quite low intensity.

Since its discovery, the Raman effect has been important as a method for the elucidation of molecular structure, for locating various functional groups or chemical bonds in molecules, and for the quantitative analysis of major components of complex mixtures. The band positions calculated from the Raman spectrum are the differences between incident and shifted frequency which only depends on the molecular structure and on the environment that surrounds it. For this reason, the shapes and positions of the Raman bands do not depend on the frequency of the exciting radiation. The same cannot be said, however, for the intensity of the scattered light which is strongly dependent on the frequency of the exciting radiation.

If the laser frequency occurs near or at the frequency of an electronic transition (see Figure 1), a very significant intensity enhancement may occur. This technique is called resonance Raman

spectroscopy (RRS); the advantage of RRS lies in its great sensitivity and selectivity as a probe of chromophore structure. The enhanced Raman lines may have intensities 10^2-10^6 times greater than normal Raman intensities. Nevertheless, its applicability is limited by the number of laser lines available and the spectrum is sometimes obscured by an intense fluorescence background.

The poor sensitivity of normal Raman scattering (NRS) has limited the use of this technique for analytical trace analysis purposes. Recently, researchers have observed an enhancement in the Raman scattering signals by factors of 10^3-10^6 when a compound is absorbed on or near special metal surfaces. This new Raman technique is known as surface enhanced Raman scattering (SERS) spectroscopy.

The Surface Enhanced Raman Effect

The first observation of the phenomenon now known as surface enhanced Raman scattering was in 1974 when Fleischmann et al. (1) were using laser Raman spectroscopy to detect adsorbed pyridine in the region of the silver-electrolyte interface in an electrochemical cell. They observed a signal larger than the one expected. However, because of the complexity of the electrochemical system, it was thought that the increased signal was due to the increased surface area and the corresponding increase in adsorbed molecules on the silver electrode because of its roughening during the anodization process. It was soon pointed out by Jeanmarie and van Duyne (2) and simultaneously by Albrecht and Creighton (3) that the enhanced signal was not due to the increase in the number of adsorbed molecules, but

to the increased Raman cross-section by a factor ranging between 10^4 and 10^6 for adsorbed molecules on the roughened silver electrode surface. Since then, an extensive amount of theoretical (4,5) and experimental work (6,7) has been reported, whose central theme is to understand how the presence of a solid surface modifies the spectroscopic and photochemical properties of a molecule located nearby.

A generally accepted explanation for this phenomenon has not yet been established, and it is most likely that the enhancement is due to the contribution of several factors. The theories developed can be divided into two groups: electromagnetic model (also termed classical, nonlocal, long range mechanism) and chemical model (also termed nonclassical, local, short range mechanism). The first is quite well understood; it involves the enhancement of the optical fields at the surface of properly roughened, free-electron like metals. Adsorbed molecules which are found at the surface demonstrate magnified optical effects, including an apparent increase in the Raman cross-section. In fact, the cross-sections need not be modified for this mechanism to operate since the effect involves an increase in the intensity of the exciting field. Because it is an electromagnetic phenomenon, there is no intrinsic requirement that the molecule be in direct, chemical contact with the substrate. For this reason, electromagnetic enhancement is sometimes referred to as long range.

On the other hand, a number of arguments have been set for an additional enhancement based on a more specific interaction of the adsorbed molecule with the metal substrate. The main points of

controversy are (i) the different behavior among different molecules, (ii) the different enhancement of different Raman bands, (iii) the dependence on adsorption geometry and (iv) the influence of experimental parameters to which the electromagnetic mechanism should be insensitive. The existence and the mechanism of a chemical enhancement, which has been postulated to explain these points, is still in much debate. Nevertheless, it has become known that the best candidates for enhancement models of this type are those involving some kind of charge transfer between the molecule and the substrate. This has been corroborated by the fact that virtually all the molecules examined successfully by SERS experiments are able and show tendency to form charge transfer complexes with noble and transition metals, since all of them possess lone-pair electrons and/or π orbitals. When this short range mechanism is present, the scattering cross-section of the adsorbed molecule is modified.

The Electromagnetic Model

Theoretical predictions of the magnitude of the electromagnetic effect depend on the boundary conditions of the model and therefore involve a dependence on the roughness of the surface. The spheroidal model proposed by Gersten and Nitzan (8) applies particularly to colloidal solutions of dielectric particles or to low coverage surface island films. They described a rough surface as being a set of protrusions which stick out of an underlying planar substrate. They assumed these protrusions to be spheroids characterized by an aspect ratio equal to a/b, where a is the semi-axis along the axis of symmetry and b is the semi-axis perpendicular to the axis of

symmetry. As shown in Figure 2, for prolate spheroids a/b > 1, while for oblate spheroids a/b < 1. In the special case a/b = 1, the spheroid degenerates into a sphere. They further assumed that the dimensions of the spheroid are small compared with the wavelength of light.

The free electrons in a metal particle oscillate at a specific frequency called the resonance frequency, determined by the particles size and shape. Oscillations can be associated with charge separation along the symmetry axes, axially symmetric oscillation mode, or charge separation perpendicular to the symmetry axis, azimuthally excited oscillation mode. Both of these oscillation modes are shown in Figure 2(b) for a prolate spheroid.

Figure 3(a) shows how the dielectric function of the metal changes as a function of the aspect ratio of the spheroid for these two oscillation modes and for oblate and prolate spheroids. In the case of a prolate spheroid, as the length a increases, the dielectric function becomes more negative for the axial oscillation mode (the polarizability increases along the symmetry axis). Thus, the restoring force needed to sustain the oscillation is weakened and the frequency of oscillation decreases, as shown in Figure 3(b). On the other hand, for an oblate spheroid the frequency of oscillation decreases for the azimuthally excited mode as the width b increases (the polarizability increases perpendicular to the symmetry axis).

The dipole moment of the spheroid, μ_s, can be defined as

$$\mu_s(\omega) = \alpha_s(\omega)\, E_0(\omega) \qquad (1)$$

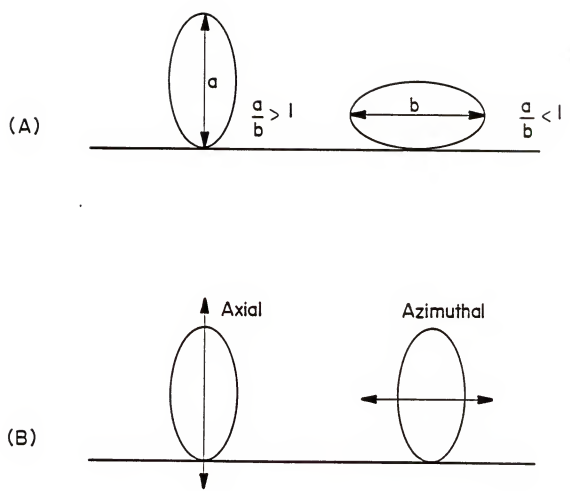

Figure 2 Schematic representations of (A) a prolate and an oblate spheroid, and (B) the axes for axial and azimuthal modes of oscillation for a prolate spheroid.

Figure 3 Dependence on the aspect ratio (a/b): (a) of the dielectric function for axially symmetric and azimuthal oscillation modes; and (b) of the plasma energies for silver spheroids. The axially symmetric mode is denoted by 1 and the azimuthally excited mode is denoted by 2.

(a)

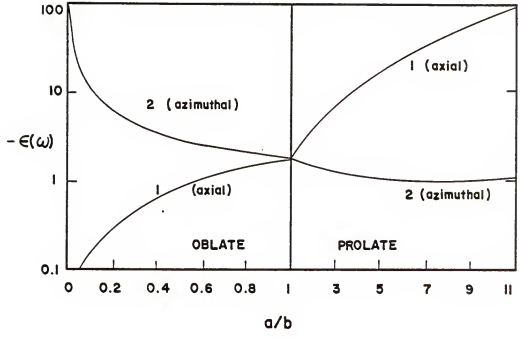
100
10
1
0.1
$-\epsilon(\omega)$
2 (azimuthal)
1 (axial)
1 (axial)
2 (azimuthal)
OBLATE
PROLATE
0
0.2
0.4
0.6
0.8
1
3
5
7
9
11
a/b

(b)

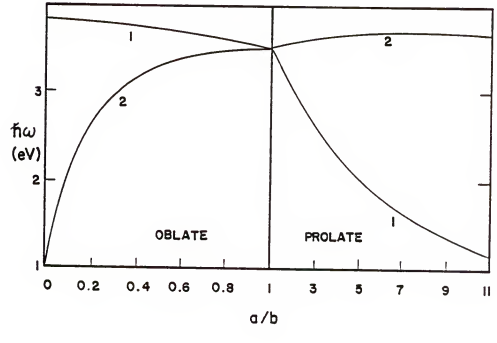
1
2
3
2
$\hbar\omega$
(eV)
2
1
2
1
OBLATE
PROLATE
0
0.2
0.4
0.6
0.8
1
3
5
7
9
11
a/b

where α_s is the polarizability of the spheroid and E_0 is the incident field strength. If the laser frequency is the same as the resonance frequency of the spheroid, a strong coupling will occur between the electric field of the incident radiation and the electric field generated by the oscillation of the free electrons in the metal (the polarization wave). Under such circumstances the dynamic polarizability of the spheroid gets to be very large and the spheroid becomes polarized even with weak incident fields. The polarized spheroid acts as a source of electric field. Therefore, as shown in equation 2, the local field in the neighborhood of the spheroid, $E(\omega)$, has two contributions to it:

$$E(\omega) = E_0(\omega) + A(\omega)E_0(\omega) \tag{2}$$

where $E_0(\omega)$ is the incident field and $A(\omega)E_0(\omega)$ is the incident field amplified by $A(\omega)$ due to the presence of the spheroid.

The Raman scattering originates from the vibrational modulation of the dipoles, $\mu(\omega)$, induced in molecules by an electric field,

$$\mu(\omega) = \alpha_m(\omega)E(\omega) \tag{3}$$

where $\alpha_m(\omega)$ is the molecular polarizability. If the scattered Raman frequency is also near the resonance frequency of the spheroid, it can similarly induce a dipole in the spheroid and become amplified by the above mechanisms. Consequently, the observed emission field, $E(\omega')$, from the Raman radiation has also two contributions to it:

$$E(\omega') = E_R(\omega') + A(\omega')E_R(\omega') \quad (4)$$

where $E_R(\omega')$ is the emission field in the absence of the spheroid and $A(\omega')E_R(\omega')$ is the amplified field due to the presence of the spheroid. The amplification factor $A(\omega')$ is now evaluated at the shifted Raman frequency ω'. Figure 4 shows how these amplified fields near the surface of a spheroid compare to the fields expected in the case of an isolated molecule.

This electromagnetic theory predicts that the enhancement will slowly decay as the distance of the molecule from the metal surface increases. It should be mentioned at this point that the surface optical resonance is well defined only for metals with favorable dielectric properties like Cu, Ag and Au. The real part of the metal dielectric function needs to be large and negative and the imaginary part very small. This characteristic is absent in Pt, Ni, Al, Hg, Cd and In meaning that, should SERS be observed with these metals, the only possible mechanism is through short range chemical communication (9).

The Short Range Mechanism--Adatom Hypothesis

Active sites at the metal surface lead to specific communication between the metal and the molecule. Otto (6) has been a strong proponent of a model of the active site. His hypothesis links the coupling between an adsorbate and the electron-hole excitations in a metal (in the case of chemisorption), to the strong photon electron-hole pair coupling caused by atomic scale roughness. It predicts

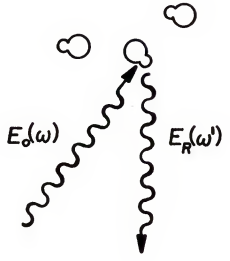

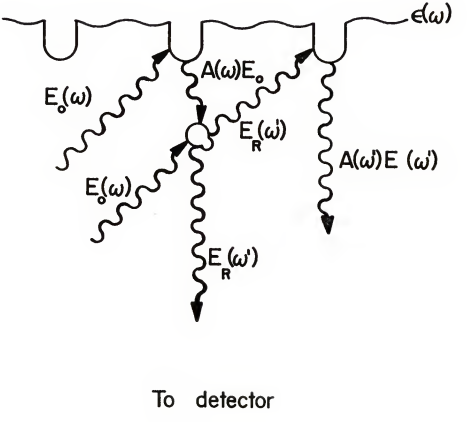

Figure 4 Comparison of Raman scattering from an isolated molecule with that of a molecule located near a metal surface.

SERS for molecules chemisorbed to adatoms or clusters of adatoms (e.g., silver adatoms on silver) and the continuous inelastic background usually observed in the SERS spectra.

In this hypothesis (10), individual adatoms of the metal substrate act as centers for the creation of electron-hole pairs in the metal, i.e., the adatom delivers the momentum necessary so that a photon can excite electron-hole pairs near the adatom of the same excitation energy as the photon energy. Once created the electron or hole will interact with the adsorbate bound to the adatom and excite an adsorbate vibration (electron-adsorbate interaction). This type of excitation is local in nature and should couple stronger with the adsorbed molecule than do the collective excitations present in surface plasmons. Several mechanisms have been proposed for the electron-hole adsorbate interaction (11). The most widely accepted is the tunneling of the electron or hole from the metal via the adatom into electronic states of the adsorbate and back into the metal. The vibrational excitation, thus, is caused by the electron-adsorbate interaction, and not by the photon-adsorbate interaction as in NRS.

Furthermore, this theory attributes the observation of a continuum background (10) to electron-electron interactions after which the electron-hole excitation left over may have any energy. Recombination of electron-hole pairs results in the observed radiative continuum (also termed electronic Raman scattering) which is present even in the absence of an adsorbate.

Two other hypotheses should also be mentioned in this section:

(i) Complex formation between the metal and the adsorbate could lead to distorted orbitals on the molecule and the possibility of enhanced scattering through the normal resonant Raman effect.

(ii) Charge transfer transitions between the molecule and the metal could change the effective polarizability of the system thus enhancing the Raman cross-sections of the adsorbate.

SERS on Metal Colloids

In addition to many studies of metal/electrolyte interfaces, SERS has been observed at metal/air interfaces, at metal/vacuum interfaces, at solid/solid interfaces, on metal colloids and on metal island films. Numerous applications of SERS to various analytes on these substrates appear in reference 7. Of the various types of particulate metal samples, however, aqueous colloidal dispersions are particularly easy to prepare by simple chemical techniques. These methods provide control of particle size and shape, quantities which can be observed and which determine the critical sensitivity of the enhancement based on the theory of the electromagnetic model. Their optical properties, particularly their absorption spectra, are easily measured and continuous renewal of the sample by flow through the light beam is possible. For these reasons, metal colloids have played an important role in the elucidation of the significance of metal plasma resonances in the surface enhanced Raman effect.

Metal Colloids

Colloids are generally considered to include particles having diameters in the range of 10^{-7} to 10^{-4} cm or those containing 10^{3} to 10^{9} atoms (12). They can be broadly classified into two main groups, namely, lyophobic and lyophilic colloids. The first group are generally dispersions of insoluble inorganic substances in a liquid medium, usually aqueous, and have little attraction for the solvent. The second group, on the other hand, traditionally consists of soluble macromolecules, in a liquid medium, which have strong affinity for the solvent. Colloidal systems owe their stability to a surface charge and the resultant electrical repulsion of charged particles. References 13 and 14 provide a comprehensive discussion on colloids and colloid stability.

Metal particles in aqueous colloidal dispersions are generally negatively charged due to the adsorption of anions present in solution. Thus, encounters between particles as a consequence of Brownian motions result in electrostatic repulsion and hence stability against aggregation. When a neutral adsorbate molecule, however, is added to the system, it replaces the adsorbed anions reducing the charge on the particles and increasing the possibility of particle adherence by attractive forces as they collide. The extent of the aggregation will depend upon the concentration of neutral adsorbate added as is apparent from the range of color changes that colloidal solutions undergo. So, at low concentrations of adsorbate, the primary particles slowly aggregate to form strings of particles rather than globular clusters of particles (a fact that will be further

discussed below) which remain dispersed. At high concentrations of adsorbate, aggregation can be rapid and lead to complete precipitation, unless the colloid is stabilized by the addition of a polymeric adsorbate which protects the particles from intimate contact on collision.

In general, particularly at low concentrations of adsorbate, the displacement of the adsorbed ions is incomplete, and the particles and growing aggregates still bear a residual charge. It is this residual charge which determines the shape of the aggregates, i.e., the formation of strings of particles, since collisions at the end of a chain of charged particles, which build up the chain, are more favored than those at the sides of the chains. The residual charge furthermore protects the chains from subsequent collapse into more compact clusters. Thus, this type of aggregation may be explained as a consequence of the opposing effects of short range attractive forces and longer range repulsive forces between the aggregating primary particles.

Finally, it should be considered at this point what induces the neutral molecule to adsorb at the surface of the metal particle. As it was pointed out by van Duyne (15), neutral molecules can adsorb just because of hydrophobic forces. In general, the less soluble an organic molecule is in the aqueous medium, the more strongly it is adsorbed. Moreover, molecules with lone-electron pairs can covalently bond to the vacant orbitals on the metal surface via these electrons. The combination of these two driving forces will account

for the adsorption of neutral molecules on the surface of metal colloids.

Analysis of Results and Theory of SERS on Metal Colloids

Surfaced enhanced Raman scattering on metal colloids was first reported by Creighton et al. (16) who studied the Raman scattering of pyridine adsorbed on silver and gold colloids. They found that the maximum in the excitation profile for the enhanced Raman scattering coincided with the extinction maximum for different colloids at various stages of aggregation. This fact was taken as a demonstration of the association of the enhancement in SERS with the resonant excitation of electron collective oscillation modes in the metal (17). A theoretical description of this contribution to the enhancement observed has been given by Kerker et al. (18) and by Gersten (19). Recently, both treatments have been extended to include the enhancement of Raman scattering by molecules at the surface of metal spheroids (8,20). Due to the mode of aggregation of the metal colloids (strings of particles instead of globular clusters of particles), there is a qualitative similarity between the treatment given to explain their optical properties and the spheroidal model used to explain the electromagnetic enhancement mechanism.

As discussed earlier, in this model the SERS effect owes its high intensity to an enhancement of the electromagnetic fields at the metal surface, due to the resonance response of the particle to the incident light and a further resonance response to the Raman scattered light. The simplified expression for the enhancement in the limiting case that the particle be much smaller than the wavelength of light

is given by

$$G = |[1 + 2g(\omega)][1 + 2g(\omega')]|^2 \qquad (5)$$

where $$g_i = \frac{\varepsilon - 1}{3[1 + (\varepsilon - 1)P_i]} \qquad i = a,b,c \qquad (6)$$

In this equation ε is the frequency dependent dielectric function of the metal relative to the surroundings and the factor P_i depends upon the values of the three semi-axes (a, b and c) of the particle. The polarizability of the particle is given by

$$\alpha_s = a\ b\ c\ g_i \qquad (7)$$

For an isolated sphere, P_i has a triply degenerate value equal to 1/3 and a = b = c; the polarizability is given by $\alpha_s = a^3 g$ and g at ω and ω' is given by

$$g(\omega) = \frac{\varepsilon(\omega) - 1}{\varepsilon(\omega) + 2} \qquad g(\omega') = \frac{\varepsilon(\omega') - 1}{\varepsilon(\omega') + 2} \qquad (8)$$

Excitation of the dipolar surface oscillations of the free electrons in the particle, which results in SERS, takes place whenever there is a resonance as the denominator of $g(\omega)$ and $g(\omega')$ become small. This happens at the frequency at which the dielectric function approaches a value of -2. At this frequency there is also an absorption and scattering maximum in the extinction spectrum of the particles.

Consider now two very small spheres of the same radius in contact; they can be treated as if they were an isolated spheroid. In this instance, P_i will have two values: one corresponding to the major axis of the spheroid and one doubly degenerate value corresponding to the other two semi-axes of the spheroid. Thus, the spheroid has two polarizability components: one in which the dipole oscillates parallel to the spheroid major axis, longitudinal polarizability; and one in which the dipole oscillates perpendicular to the spheroid major axis, transverse polarizability, given by

$$\alpha_\ell = \frac{8a^3}{3}\left(\frac{\varepsilon - 1}{\varepsilon + 3}\right) \qquad P_a = \frac{1}{4} \tag{9}$$

and

$$\alpha_t = \frac{16a^3}{3}\left(\frac{\varepsilon - 1}{3\varepsilon + 5}\right) \qquad P_{b \text{ or } c} = \frac{3}{8} \tag{10}$$

The pair of spheres shows a longitudinal and a transverse resonance at the frequencies at which $\varepsilon = -3$ and $\varepsilon = -5/3$, respectively. The triply degenerate absorption band for the sphere now splits into two bands, which depend upon the two semi-axes of the spheroid. This is demonstrated in Figure 5(a); the lower wavelength absorption band corresponds to the excitation of the transverse oscillation mode of the spheroid. As aspect ratio of the spheroid increases this band remains at roughly the same wavelength. The second band in the absorption spectra shown in Figure 5(a) corresponds to the excitation of the longitudinal oscillation mode, this band

Figure 5 Graphical representations: (a) of the calculated extinction cross-section for silver prolate spheroids in water for various axial ratios; and (b) of the calculated enhancement for a 1010 cm^{-1} Raman band as a function of excitation wavelength for a monolayer of adsorbate on silver prolate spheroids in water for various axial ratios. Curves denoted 1 through 5 correspond to an aspect ratio of 1.0, 1.5, 2.0, 2.5 and 3.0, respectively.

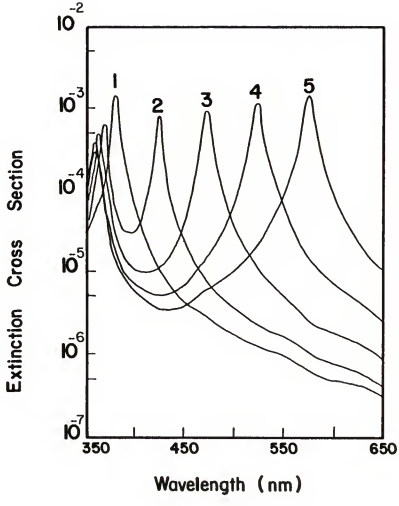
Extinction Cross Section
10^{-2}
10^{-3}
10^{-4}
10^{-5}
10^{-6}
10^{-7}
1
2
3
4
5
350
450
550
650
Wavelength (nm)

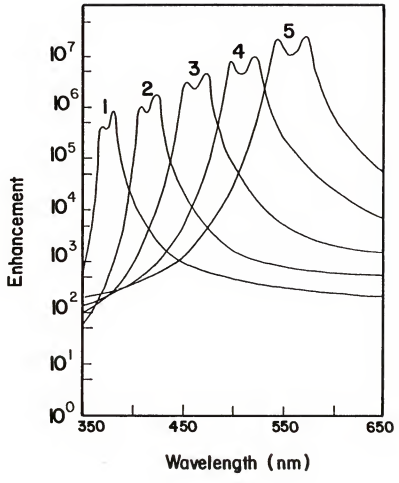
Enhancement
10^{7}
10^{6}
10^{5}
10^{4}
10^{3}
10^{2}
10^{1}
10^{0}
1
2
3
4
5
350
450
550
650
Wavelength (nm)

moves to longer wavelengths when the aspect ratio of the spheroid increases. Figure 5(b) shows the excitation profiles of a Raman band as the aspect ratio of the spheroid increases. The maximum enhancement increases in magnitude and shifts toward longer wavelength as a/b increases; in all cases the excitation maximum corresponds to resonant excitation of the longitudinal oscillation mode of the spheroid.

It has been demonstrated (21,22) by transmission electron micrograph (TEM) experiments that, upon addition of an adsorbate to a metal colloidal suspension, the particles aggregate forming strings that resemble an elongated spheroid. Careful studies on copper, gold and silver hydrosols (20,23,24) have demonstrated that for all three the excitation profile for SERS peaks at the same wavelength as the second absorption band of their extinction spectra. These results are shown in Figure 6 for pyridine adsorbed on a gold hydrosol at different stages of the aggregation process. Excitation under the transverse resonance, however, does not produce any detectable Raman scattering from the adsorbate. This behavior may be understood qualitatively in terms of the greater change in polarizability (dielectric function becomes large and negative) that the spheroid will experience when the dipole plasma along its major axis is excited as compared to when it is excited along its minor axis. The SERS intensity is approximately given (25) by

$$I = \text{const} \left[\frac{|\varepsilon_0|^2 |\varepsilon_R|^2 \lambda_0 \lambda_R}{(\varepsilon_2)_0 (\varepsilon_2)_R}\right] A_0 A_R \qquad (11)$$

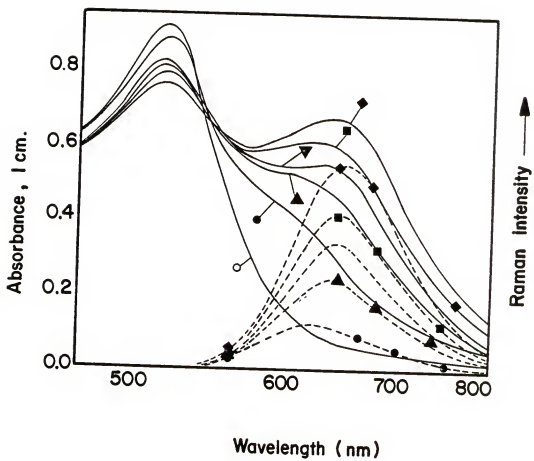

Figure 6 Experimental extinction (——) and excitation profiles (---) for the 1014 cm^{-1} band of pyridine on gold hydrosols. (○) indicates before and (●) 11 hr, (▲) 25 hr, (▼) 35 hr, (■) 49 hr and (◆) 73 hr after adding pyridine.

where A_0 and A_R are the fractional absorbances and $\varepsilon_0 = (\varepsilon_1)_0 + i(\varepsilon_2)_0$ and $\varepsilon_R = (\varepsilon_1)_R + i(\varepsilon_2)_R$ are the metal dielectric functions at the excitation and Raman scattered wavelengths, respectively. At resonance the real part of the dielectric function, ε_1, becomes large and negative while the imaginary part, $i\varepsilon_2$, becomes small and negligible. Equation 11 shows that, for small Raman shifts, the Raman intensity becomes approximately proportional to the square of the absorbance of the colloids at the excitation wavelength used.

Finally, three remarks about this theory must be made:

(i) It only applies for particles much smaller than the wavelength of light for which the elastic scattering of the exciting radiation contributes less than 5% to the total extinction spectrum of the spheroids (21). Therefore, the bands observed in such spectra are mostly absorption bands arising from the resonance excitation of the spheroids' oscillation modes.

(ii) For larger particles, the theory no longer applies, as one is dealing with a superposition of multipolar fields rather than with dipolar fields. Under such circumstances, the absorption and scattering spectra of the spheroid will be decoupled from the SERS excitation spectrum.

(iii) A more rigorous electrodynamic model should also consider the dipole coupling between the plasma modes of adjacent spheroids.

CHAPTER THREE
A SIMPLE DEVICE FOR SERS STUDIES

Introduction

The scattering cross-sections in NRS spectroscopy are very low, typically of the order of 10^{-30} cm^2. It is very difficult to detect these weak signals in the presence of stray light from the unshifted laser wavelength which often causes an intense background. For this reason, Raman spectroscopy has been almost invariably done with big (focal length, f ~ 1 m) double and triple monochromators which provide large stray light rejection even at wavelengths very close to the Rayleigh line. In this way, the achievable signal to noise ratio depends mostly on the pump intensity and on the sensitivity of the detection device. However, using high power lasers brings about another problem which is sample decomposition.

The newly developed SERS technique provides enhancements up to six orders of magnitude. This fact could allow the scientist to observe Raman bands even above relatively high background signals. In fact, when resolution is of secondary importance, greater signal to noise ratios, S/N, could be obtained by using a monochromator of smaller focal length than the conventional ones used for Raman spectroscopy. It is appropriate at this point to discuss some basic parameters of importance in the characterization of a monochromator.

Theoretical Concepts

There are two basic properties that determine the performance of a monochromator for a given application (26,27,28). These are spectral resolving power, which specifies the minimum separation between two lines that can just be resolved, and étendue or light gathering power, which determines the capability of the monochromator to gather as much radiation from the source as possible. Unfortunately, these are two conflicting requirements, and the best compromise between them is desirable. For the discussion that follows to be valid, several assumptions are necessary:

(i) the focal length, f(mm), of the collimating and focusing elements of the monochromator are equal;

(ii) the width, W(μm), of the entrance and exit slits of the monochromator are equal and homogeneously illuminated;

(iii) diffraction effects and optical imperfections are ignored.

Resolution and Resolving Power

The attainable spectral resolving power of a monochromator is determined by its angular dispersion $d\theta/d\lambda$ which denotes the difference in the emergent angle, $d\theta$ (rad), of two dispersed beams separated by a wavelength difference of $d\lambda$ (nm). The linear dispersion $ds/d\lambda$ (μm/nm) denotes the geometrical distance ds (μm) between the images formed at the focal plane by the two beams with wavelength difference $d\lambda$. If the focal length of the focusing element of the monochromator is f (mm), the linear dispersion at the focal plane is

$$\frac{ds}{d\lambda} = f \frac{d\theta}{d\lambda} \tag{12}$$

The range of wavelengths of radiation emerging from the exit slit of a monochromator when polychromatic radiation is incident upon the entrance slit given by

$$\Delta\lambda_S = W \frac{d\lambda}{ds} = \frac{W}{f} \frac{d\lambda}{d\theta} \tag{13}$$

where $\Delta\lambda_S$ (nm) is called the spectral bandpass which is defined as the product of the slit width W (μm) and the reciprocal linear dispersion $d\lambda/ds$ of the monochromator.

The resolving power R of monochromator is defined by

$$R = \frac{\bar{\lambda}}{\Delta\lambda_R} \tag{14}$$

where the resolution, $\Delta\lambda_R$, is the wavelength difference (nm) between two monochromatic spectral lines which can be "just barely" distinguished as separate lines and $\bar{\lambda}$ is the mean wavelength of the two lines. The exact definition of resolution depends upon the criterion for separation; however, in any case $\Delta\lambda_R > \Delta\lambda_S$ (usually $\Delta\lambda_R = 2\Delta\lambda_S$).

Light Gathering Power

When a continuum source of radiation is placed in front of a monochromator, the decisive quantity of the source is the spectral radiance expressed in watts per unit of surface, per unit of solid

angle and unit of wavelength. On the other hand, the photomultiplier detector (PMT) responds to the radiant flux, Φ, in watts, emerging from the exit slit of the monochromator:

$$\Phi = B_{c\lambda_0} WHT_f \Omega \Delta\lambda_s \tag{15}$$

where Φ = total flux emerging from exit slit, W

$B_{c\lambda_0}$ = spectral radiance of a continuum source, W cm^{-2} sr^{-1} nm^{-1}

T_f = transmission factor of optical system, dimensionless

W = illuminated width of slit, cm

H = illuminated height of slit, cm

Ω = solid angle of light collected by the spectrometer, sr

$\Delta\lambda_s$ = spectral bandpass of monochromator, nm.

Therefore, the monochromator introduces a proportionality factor with the dimensions of a solid angle, times a wavelength interval, times a surface area, and this factor should be as large as possible. The solid angle, Ω, is given by

$$\Omega = \frac{A}{f_c^2} \tag{16}$$

where A is the area of the limiting aperture (cm^2) and f_c the focal length (cm) of the collimator lens. The product U = ΩHW is often called étendue.

Signal to Noise Expressions

The analyte signal for any spectrometer in terms of photocathodic counts is given (29) by

$$S = B_{PC}\ \Omega\ A\ T_f\ Q\ \Delta\lambda_s\ t_0 \tag{17}$$

In the present discussion, the signal will be assumed to originate in a continuum source and in the presence of a background, B, which produces a spectrally broad signal given by

$$S_B = B_{PB}\ A\ \Omega\ T_f\ Q\ \Delta\lambda_s\ t_0 \tag{18}$$

where B_{PC} = photon spectral radiance of continuum source, photons s^{-1} cm^{-2} sr^{-1} nm^{-1}

B_{PB} = photon spectral radiance of background radiation, photons s^{-1} cm^{-2} sr^{-1} nm^{-1}

Q = photocathode efficiency, dimensionless

T_f = transmission factor, dimensionless

A = area of entrance slit, cm^2

Ω = solid angle filled by source (and background) and transferred to spectrometer, sr

t_0 = observation time per spectral interval (bandpass), s

$\Delta\lambda_s$ = spectral bandpass, nm.

The noise expressions for background shot noise and detector shot noise limited conditions are

$$N_{BS} = (S_B\ t_0)^{1/2} \tag{19}$$

$$N_{DS} = (R_D\ t_U)^{1/2} \tag{20}$$

where R_D = detector dark counts/s. In the comparison to follow, t_m will be designated as the total measurement time and ℓ is the total number of spectral components. The S/N expressions for a single slit, single detector, linear scan grating monochromator are

(i) for the detector noise limitation

$$\frac{S}{N} = B_{PC}\ A\ \Omega\ T_f\ Q\ \Delta\lambda_s\ \left(\frac{t_m}{R_D \ell}\right)^{1/2} \tag{21}$$

(ii) for the background shot noise limitation

$$\begin{aligned}\frac{S}{N} &= \frac{B_{PC}\ A\ \Omega\ T_f\ Q\ \Delta\lambda_s}{(B_{PB}\ A\ \Omega\ T_f\ Q\ \Delta\lambda_s)^{1/2}}\ \left(\frac{t_m}{\ell}\right)^{1/2} \\ &= \frac{B_{PC}}{B_{PB}^{1/2}}\ \left(\frac{A\ \Omega\ T_f\ Q\ \Delta\lambda_s\ t_m}{\ell}\right)^{1/2} \\ &= \frac{K_s}{(K_B)^{1/2}}\ t_U^{1/2}\end{aligned} \tag{22}$$

Experimental Section

Instrumentation

Two Raman systems were used for this study. The arrangement scheme of one of them is shown in Figure 7. It consisted of an Argon ion laser (Model 171, Spectra-Physics), illuminating homogeneously the entrance slit of a single-beam sample compartment from the Fluorolog 2 series spectrofluorometers (Spex Industries). The sample compartment

Figure 7 Experimental arrangement for SERS studies. M = mirrors, P = polarizers, SB = Soleil-Babinet compensator and PMT = photomultiplier tube.

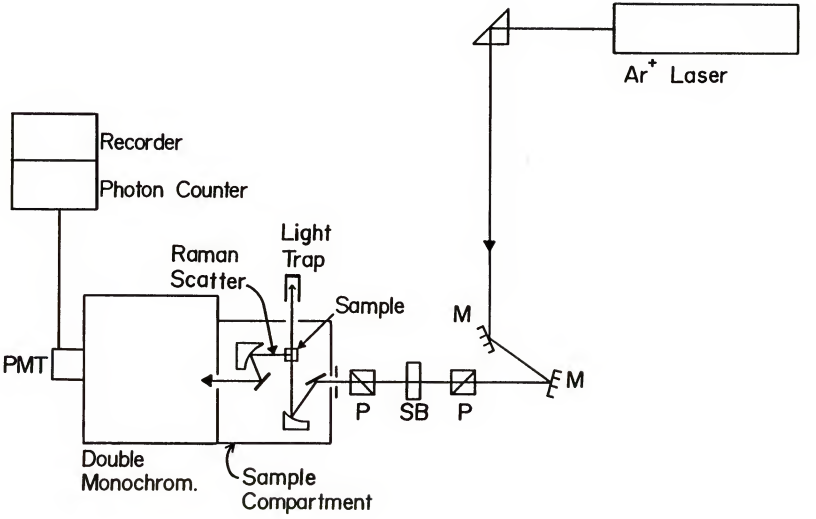
Ar+ Laser
Recorder
Photon Counter
Light
Trap
Raman
Scatter
Sample
M
PMT
M
P
SB
P
Double
Monochrom.
Sample
Compartment

was mated to a double monochromator (Model 1680B, Spex Industries) which was driven by a controlled module (Model CD2A, Spex Industries).

The polarization of the laser was changed with a Soleil-Babinet compensator (Model K1148, Karl-Lambrecht Corp.) and chosen to be perpendicular to the direction of observation by a couple of Glan-Foucault polarizers (Karl-Lambrecht Corp.). For all measurements, the intensity of the 514.5 nm laser line was 500 mW at the laser head, resulting in 100 mW reaching the sample due to transmission losses. The Raman scattered signals were collected at 90° to the excitation beam and measured with a thermoelectrically cooled (by a refrigerated chamber, Model TE 177RF-005, Products for Research, Inc.) photomultiplier tube (R-928, Hamamatsu) operated at 800V and a photon counting system (Model 1105/1120, SSR Instruments, Inc.). The samples were placed in standard 1 cm liquid sample cells.

The experimental arrangement of the second system was very similar to the one shown in Figure 7. The sample, however, was placed directly in front of the entrance slit of the monochromator. The double monochromator was replaced by a conventional one for Raman studies (Jobin-Yvon U-1000, Instruments S.A., Inc.) driven by a controller (Spectra Link, Instruments S.A., Inc.) which also provided a photon counting module for data acquisition from the photomultiplier. The optical arrangement in front of the sample was the same as in Figure 3 and the laser intensity (514.5 nm) was also 100 mW at the sample.

Procedure

Table 1 contains a list of the suppliers of the reagents used throughout this study. The silver hydrosols were prepared according to the procedure previously described by Creighton et al. (16). Typically, 20 mL of $1X10^{-3}$ M of $AgNO_3$ were added dropwise to 60 mL of vigorously stirred (ice cooled) $2X10^{-3}$ M $NaBH_4$ aqueous solution to yield a light yellow colloid which slowly turned brownish at around 15°C while it was reaching room temperature. It is very important that the colloid does not appear to be turbid when viewed under oblique illumination as this is an indication of particles which have grown to diameters greater than 50 nm. Their appearance should be that of colored solutions. The cleanliness of the glassware and purity of the materials used are important factors which determined the reproducibility and stability of the colloids. For this reason, all the glassware used for the sols had been previously soaked in a 1:1 HNO_3:H_2O solution and rinsed several times with deionized water (Barnstead Sybron Co.). All the solutions were made with triply-distilled water.

Stock solutions of 500 μg/mL of the analytes listed in Table 1 were prepared in ethanol (except for uracil, uridine and 6-amino uracil for which triply-distilled water was used). For Raman measurements, the sols were aged for two hours after which the necessary volume of analyte needed to give the desired concentration in sols was added to it. After standing for 30 min, the mixture was ready for experimental study. Hydrosols older than three hours were not used.

Table 1 List of Reagents.

Reagent	Supplier
$AgNO_3$	Fisher Scientific Co., Fair Lawn, NJ
$NaBH_4$	Eastman Kodak, Rochester, NY
CCl_4	Fisher Scientific Co., Fair Lawn, NJ
Phenytoin	Gift from Dr. S.G. Schulman, School of Pharmacy, Univ. of Florida, Gainesville, FL
PABA	Fisher Scientific Co., Fair Lawn, NJ
Uracil	Sigma Chemical Co., St. Louis, MO
Uridine	Nutritional Biochemical Corp., Cleveland, OH
6-Amino uracil	Nutritional Biochemical Corp., Cleveland, OH
Naphthalene	Mallinckrodt Chemical Works, St. Louis, MO
2-Naphthol	Eastman Kodak, Rochester, NY
2-Aminonaphthalene	Aldrich Chemicals, Milwaukee, WI
Fluorene	Eastman Kodak, Rochester, NY
2-Aminofluorene	Nutritional Biochemical Corp., Cleveland, OH
Polyvynil alcohol	Eastman Kodak, Rochester, NY
Cetylpyridinium chloride	Sigma Chemical Co., St. Louis, MO
Sodium dodecylsulfate	Sigma Chemical Co., St. Louis, MO

A Comparison Between Two Instruments

The specifications of the two monochromators used in this study are given in Table 2. In order to compare their performances, the 459 cm^{-1} Raman band of CCl_4 was scanned on both instruments as shown in Figure 8. For this band, the signal to noise ratio is determined by detector shot noise and therefore equation (21) applies. Furthermore, as mentioned in the preceeding chapter, the SERS spectra are characterized by a continuum background radiation not due to the Rayleigh line. Figure 9 shows such a spectrum for phenytoin made 1 µg/mL in the hydrosols. The signal to noise ratio in this case is background shot noise limited and thus equation (22) applies. Consequently, from Figures 8 and 9, one can calculate the signal to noise ratios (S/N) as well as the signal to background ratios (S/B) under both sets of conditions so as to evaluate which instrument is more suitable for a specific application, such results appear in Table 3.

The measurement of the full width at half maximum for the CCl_4 Raman band appeared to be 1.4 times better with the Jobin-Yvon monochromator than with the Spex. Such a result is in accordance with the manufacturer's specifications shown in Table 2. Resolution, however, is increased at the expense of light gathering power. This fact is proven by comparing S/N for both instruments. From Table 3, it is estimated that a S/N four to five times better, depending upon the type of noise limitation, can be obtained when using the Spex monochromator instead of the Jobin-Yvon monochromator. Furthermore, more rapid measurements can be done with the Spex monochromator as

Table 2 Specifications of the Monochromators Studied.

	dλ/ds (cm/μm)	f (mm)	smallest W (μm)	At 514.5 nm(a) $\Delta\nu_s$(c) (cm^{-1}, W=100μm)	At 527 nm(b) $\Delta\nu_s$ (cm^{-1})
Model 1680B Spex Industries	$1.3X10^{-10}$	220	100	6.67	6.48 (W=100μm)
Jobin-Yvon Model U1000 Instruments S.A.	$2.44X10^{-11}$	1000	5	0.92	4.4 (W=500μm)

(a) Output wavelength of Ar^+ laser.

(b) 459 cm^{-1} Raman band of CCl_4.

(c) $\Delta\nu_s = D_L^{-1}W$ where $D_L^{-1} = \frac{d\nu}{ds} = \frac{d\lambda}{dx}\left(\frac{1}{\lambda^2_{max}}\right)$, $\Delta\nu_s$ is the spectral bandpass in cm^{-1} units.

Figure 8 Scan of the 459 cm^{-1} Raman band of CCl_4: (A) with the Model 1680B from Spex Industry; and (B) with the Jobin-Yvon Model U1000 from Instruments S.A.

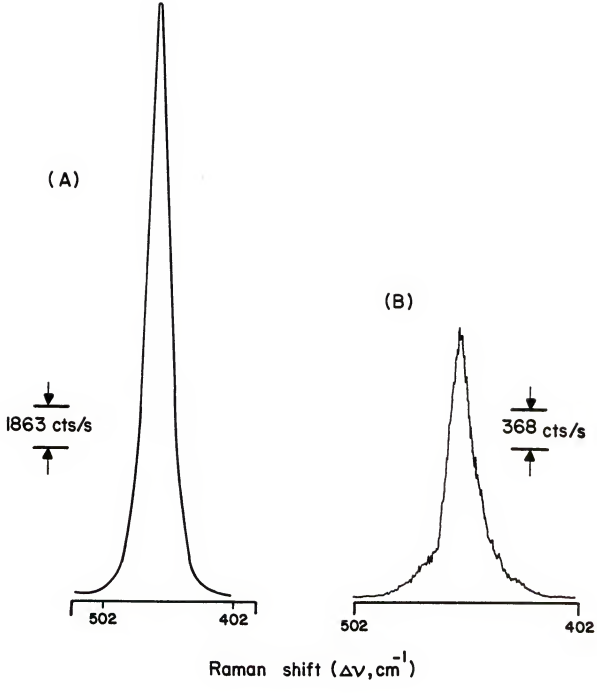
(A)
1863 cts/s
502
402
(B)
368 cts/s
502
402
Raman shift (Δν, cm⁻¹)

Figure 9 Scan of the 1005 cm^{-1} Raman band of phenytoin made 1 µg/mL in the silver sols. (A) and (B) as in Figure 8.

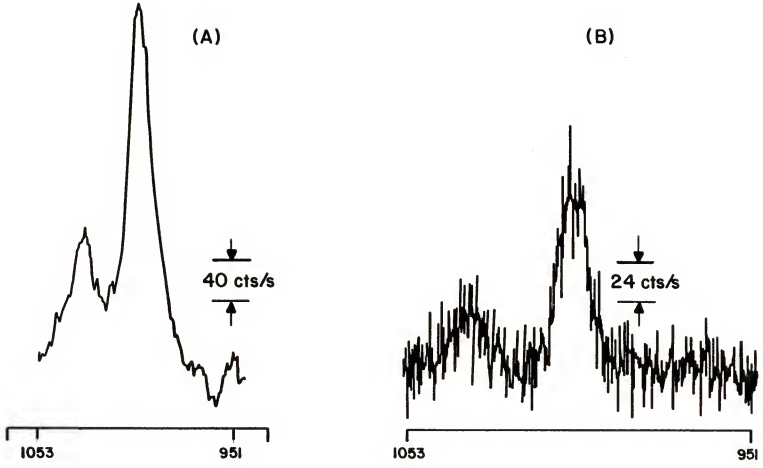
(A)
40 cts/s
1053
951
(B)
24 cts/s
1053
951
RAMAN SHIFT (Δν, cm⁻¹)

Table 3 Comparison of the Results Obtained with the Monochromators Studied.

	Scan Speed	459 cm^{-1} band of CCl_4			1005 cm^{-1} band of phenytoin	
	(cm^{-1}/min)	FWHM(cm^{-1})(a)	S/N(b)	S/B(c)	S/N	S/B
Model 1680B Spex Industries	200	18	2832	98.0	48.0	1.42
Jobin-Yvon Model U1000 Instruments S.A.	11	13	529.0	212	12.8	1.46

(a) Full width at half maximum.

(b) Signal to noise ratio, noise calculated as 1/5 peak to peak.

(c) Signal to background ratio.

it scans 18 times faster than the Jobin-Yvon. It is true that this could be improved by changing the appropriate parameters in the Jobin-Yvon system, but this would result in even smaller S/N than the ones calculated above.

Various advantages of using the smaller Spex system can be addressed at this point. First of all, the Spex system is roughly three times less expensive than the Jobin-Yvon. For the SERS studies, in which large signals limited by background shot noise are observed, an improvement in the measured S/N can be obtained at the expense of a small loss in resolution. A very large gain in measurement time is also obtained, this being a very important parameter to consider when developing an analytical technique. To further demonstrate that indeed the background limiting the signal was not coming from the laser line, the S/B for both systems was calculated and appears in Table 3. Both calculated ratios are very similar in value for the phenytoin band. If the background in the hydrosols samples was from the laser line, a bigger S/B would be expected when using the Jobin-Yvon system as this offers a much larger stray light rejection power than the Spex system. This indeed is the case for the S/B calculated for the CCl_4 band where the background is coming from the laser line.

CHAPTER FOUR
ANALYTICAL APPLICATIONS OF SERS ON SILVER COLLOIDS

Introduction

Most of the previous SERS research has been dedicated to the understanding of the phenomenon itself. Little attention has been given to the development of the technique as an analytical method for the identification and quantitation of molecular species present at trace concentration levels. Recently, however, Pemberton and Buck (30) reported the detection of a low concentration of the anion diphenylthiocarbazone adsorbed at the surface of a silver electrode. By taking advantage of the multiplicative effects of surface enhancement and resonance enhancement, concentrations as low as 10^{-9} M were reported to give spectra with acceptable S/N ratios. Following this line, Tran (31) reported subnanogram detection of dyes spotted on filter paper which was previously treated with colloidal silver hydrosols. Detection limits were in the picogram range level and the calibration plots exhibited a linear response with their slopes close to unity.

Vo-Dinh et al. (32,33) and Meier et al. (34), however, have directed their research towards the development of practical substrate materials that can be easily prepared and that can provide data with sufficient reproducibility and accuracy for analytical purposes.

Enlow et al. (35) have also applied the technique for the detection of nitro-polynuclear aromatic hydrocarbons. Specific applications of SERS as an analytical technique include the determination of copper and zinc phthalocyanine complexes on silver island films (36) and of tributyl phosphate after adsorption on silver hydrosols (37). Finally, more recently Sheng et al. (38) have studied the effects of classifying the silver hydrosols by sedimentation upon the SERS signal observed.

As an extension for these studies additional qualitative and quantitative SERS results are presented in this chapter for several adsorbates on silver colloidal hydrosols. Moreover, the data reported here reinforces the applicability of the simple and inexpensive device discussed in the previous chapter for SERS studies.

Experimental

All the SERS spectra were obtained with the experimental arrangement shown in Figure 7. All the instrumental parameters as well as procedure followed the preparation of the hydrosols and the analyte samples discussed in Chapter Three. The extinction spectra were measured with a Perkin-Elmer (Model 330) UV-visible spectrophotometer. The depolarization ratios ($p = I_a/I_b$) were calculated by rotating the polarization direction of the incident laser beam and measuring the Raman intensity when it was perpendicular (I_b) and parallel (I_a) to the direction of observation.

Results and Discussion

Characterization of Silver Hydrosols

After a stabilization period (30-60 min), the final color of the colloids was a clear solution-like brownish-yellow. Assuming all the silver ions initially added to the aqueous BH_4^- solution were reduced, the concentration of Ag° in solution is $2.5X10^{-4}$ M. As shown in Figure 10, the colloids showed a single maximum in their extinction spectrum at around 400 nm, characteristic of particles with an average diameter close to 20 nm (17,39,40). This band appears to be relatively narrow, although skewed to the right, indicating relatively little polydispersivity in the size distribution of the particles. In the absence of analyte, the colloids were stable for several weeks.

Upon the addition of the analyte, the colloids started to aggregate and a new band appeared in their extinction spectrum at the longer wavelength side of the single particle absorption band. This was accompanied by a change in the color of the sols with time, from yellow to orange, red, purple and finally gray. The effect of analyte addition in the colloid absorption spectrum is shown in Figure 11 for phenytoin added to a final concentration of 1 µg/mL in the sols. As the colloid progressively changed color with time, the new band moved to longer wavelengths as it is apparent from the spectra shown in Figure 12. The kinetics of this process depends upon the aging period of the colloids used and the type of analyte as well as the concentration added. It will be shown that this is an important factor to consider when using this technique for quantitation studies.

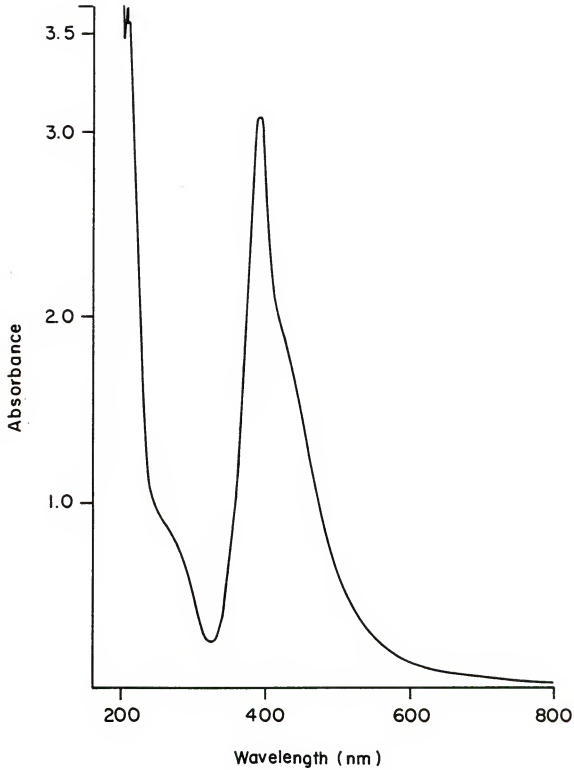

Figure 10 Absorption profile of silver hydrosols.

Figure 11 Absorption profile of silver hydrosols 30 min after adding phenytoin to a final concentration of 1 μg/mL.

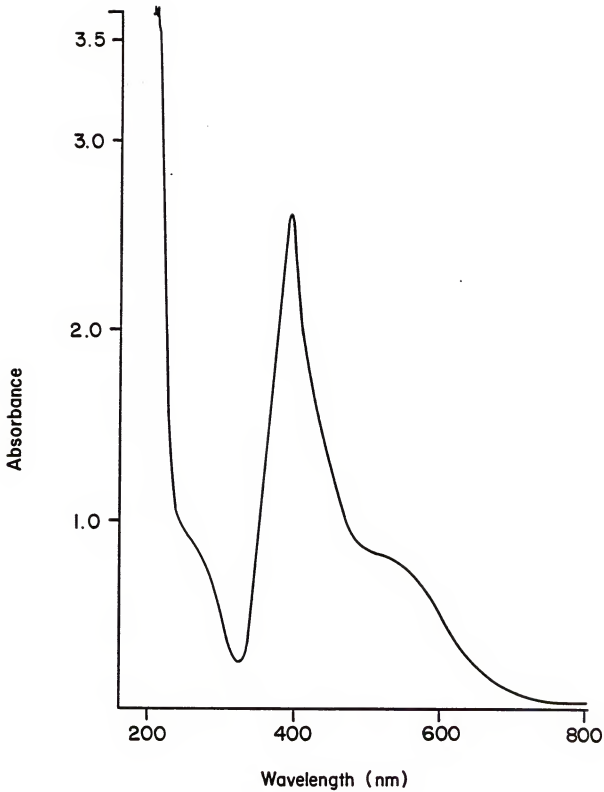
3.5
3.0
2.0
1.0
Absorbance
200
400
600
800
Wavelength (nm)

Figure 12 Absorption profile of silver hydrosols after adding phenytoin to a final concentration of 1 μg/mL, a-f taken successively every 10 min.

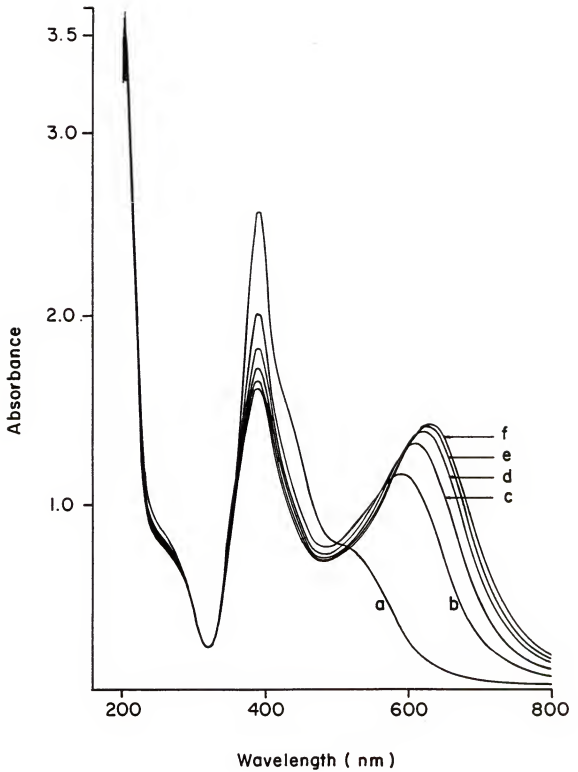
3.5
3.0
2.0
1.0
Absorbance
200
400
600
800
Wavelength (nm)
a
b
c
d
e
f

Finally, Figure 13 shows the effect upon analyte addition on the absorption spectrum for colloids that were aged for 24 hours, instead of two hours as in Figure 12. The first feature to notice is that 50 times more analyte was needed in order to produce an effect comparable to the one shown in Figure 12. The spectra follow the same trend as those in Figure 8, with the difference that the second maximum always peaks at shorter wavelengths. This indicates that the particles are aggregating into shorter strings and to a lower extent (since more analyte was needed) as should be expected for a more stable colloidal solution.

Qualitative Study

In order to assess the identification power of the SERS spectra obtained with the instrumental system described in Chapter Three, several adsorbates were studied. The molecular structures of the first group of adsorbates analyzed appear in Figure 14. These are pyrimidine derivatives of ribonucleic acid (RNA) and the amino derivative of one of them. The technique of SERS spectroscopy has been advantageously used for the study of nucleic acid components. The advantages include small sample requirement, minimal sensitivity towards interference by water, spectral detail, and conformational and environmental information.

In the past, researchers have successfully studied the SERS spectra of nucleic acid components of deoxyribonucleic acid (DNA) and some of their derivatives at rough silver electrode surfaces (41-44) and on colloidal silver suspensions (45-47) at concentration levels as

Figure 13 Absorption profile of silver hydrosols after adding phenytoin to a final concentration of 50 µg/mL, with silver hydrosols aged for 24 hr before adding phenytoin.

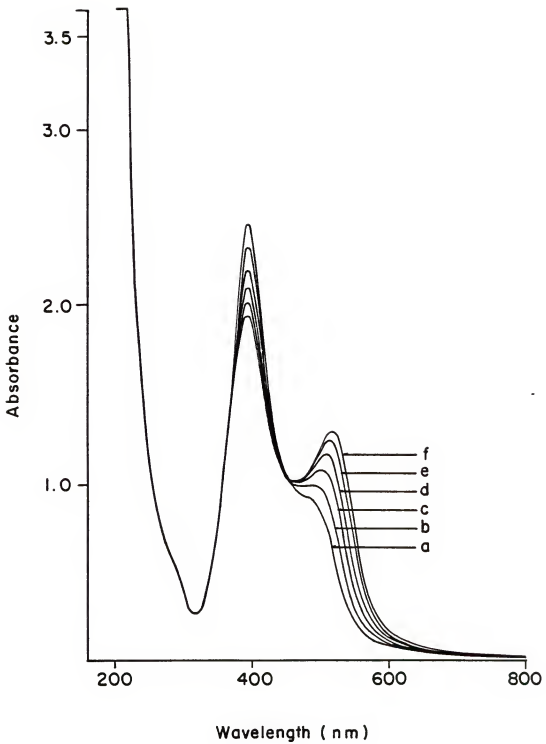
3.5
3.0
2.0
1.0
Absorbance
200
400
600
800
Wavelength (nm)
f
e
d
c
b
a

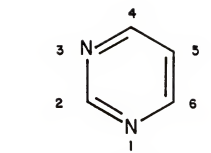

pyrimidine

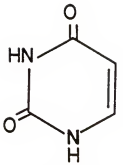

uracil

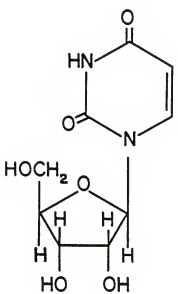

uridine

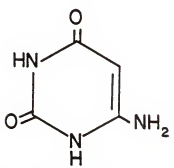

6-amino uracil

Figure 14 Molecular structures of pyrimidine derivatives in ribonucleic acid: uracil and uridine, and 6-amino uracil.

low as a few μg/mL. Of the N-containing bases of RNA, uracil is the only one which is not present in DNA (thymine takes its place). Although its biological importance in the process of protein synthesis is clear, its SERS spectrum has not yet been reported in the literature.

The SERS spectrum of uracil is shown in Figure 15. The band positions together with their vibrational mode assignments appear in Table 4. Due to the very low NRS and to the experimental arrangement used in this study, no spectrum could be observed for the molecule when dissolved in water. For comparison purposes, however, the data obtained from reference 44 for thymine in water are included in Table 4. Furthermore, normal mode calculations have previously been performed (48) for uracil and these are included in the table as well and are used for the assignments.

In the ring bending mode region, only two bands appear at 578 and 603 cm^{-1}. Four other bands have been reported (44) at lower energies, but in this study the intense Rayleigh line prevents their observation. At 796 cm^{-1}, the totally symmetric ring stretching vibration appears. It agrees very well with the calculated value of 795 cm^{-1}. It is known from NRS that this mode, common to all pyrimidines, is particularly insensitive to changes in the chemical surroundings. This band is the most prominent SERS band in the spectrum as has been the case for other nucleic acid bases adsorbed on silver colloids (46). In addition to its high intensity, this band was also found to have a high depolarization ratio ($\rho > 0.75$), whereas

Figure 15 Scattered intensity (1 cm = 130 cts/s) vs. Raman shift ($\Delta\nu$, cm^{-1}) of (a) 500 μg/mL uracil in water; (b) the silver hydrosols showing the continuum background radiation; and (c) 5 μg/mL uracil in silver hydrosols (SERS spectrum).

RELATIVE SIGNAL INTENSITY
RAYLEIGH LINE
578
603
796
1040
1207
1267
1381
1511
1582
1610
(c)
(b)
(a)
1800
600
RAMAN SHIFT (Δν, cm⁻¹)

Table 4 SERS Results for Uracil.[a]

$\Delta\nu_{Ag}$[b]	$\Delta\nu_{Ag}$[c]	$\Delta\nu_{H_2O}$[d]	Calculated[e]	Line shift[f]	Assignments
578 (.20)	586	565		13	$N_1C_2N_3^B - C_2N_3C_4^B$
603 (.20)	632		614		$N_1C_2O^B + N_3C_4O^B$
796 (1.0)	776	750	795	46	Ring breathing
1040 (.13)					Stretching motion of the ring's
1094 (.11)					C-N bonds[h]
1207 (.40)	1184	1169	1200	7	$-C_6H^B + C_2N_3^S$
1267 (.49)	1275	1238		29	$Ring^S + CH^B$
1381 (.50)	1344	1360	1375	21	$N_3H^B - C_4 = O^S$
1511 (.23)	1504	1503		8	NH^B
1559 (.07Sh)	1562				
1582 (.11)	1584	(g)	1562		$N_3C_4^S + N_1C_2^S + C_6H_5^S - N_1C_6^S$
1610 (.30)	1652	1657		-47	$C_4 = O^S + C_5 - C_6^S$
		1691			$C_2 = O^S$

Table 4--continued.

(a) Abbreviations used: S = stretching, B = bending, Sh = shoulder.

(b) SERS in this study, values in parentheses are relative intensities.

(c) SERS from reference 44.

(d) NRS from reference 44.

(e) Calculated values from reference 48.

(f) Line shift = $\Delta\nu_{Ag}^{(b)} - \Delta\nu_{H_2O}^{(d)}$.

(g) Could not be seen due to solvent interference.

(h) From reference 49.

for aqueous uracil the corresponding band is almost completely polarized ($\rho \leq 0.25$) (49). This fact suggests that the molecule is actually adsorbed on the silver surface.

In the SERS spectrum, a band appears at 1267 cm^{-1} which can be assigned to a combination of bending and stretching modes, i.e., ring stretching + CH bending. Only a weak line can be seen in the single bond stretching region at 1511 cm^{-1}. In the double bond stretching region, three lines are observed at 1559, 1582 and 1610 cm^{-1}. The band at 1559 could not be identified in accordance with reference 44. The band at 1582 can be assigned to the $N_3C_4(s) + N_1C_2(s) + C_6C_5(s) - N_1C_6(s)$ vibration. The line at 1610 cm^{-1} is assigned to a carbonyl stretching mode. Although in uracil, two carbonyl stretching modes are expected, only one is seen. Otto et al. (44) have suggested that the band at 1610 cm^{-1} arises from one mode only, which most likely is the C_4=O mode. This band is shifted to a lower frequency by 47 cm^{-1}. Electron donation of this group to the surface would decrease the bond order, resulting in a decrease in the vibrational frequency. It seems likely, then, that uracil coordinates to the surface through this group and that the molecular plane is perpendicular to the surface instead of being parallel to it because, in that case, there would be no difference between the orientation of the different carbonyl groups.

Table 5 and Figure 16 show that the Raman spectra of uracil and uridine are very similar. This is because the Raman lines of ribose are very weak compared to those of the pyrimidine nucleus. Two new

Figure 16 Scattered intensity (1 cm = 130 cts/s) vs. Raman shift ($\Delta\nu$, cm^{-1}) of (a) 500 μg/mL uridine in water; (b) the silver hydrosols; and (c) 5 μg/mL uridine in silver hydrosols (SERS spectrum).

RELATIVE SIGNAL INTENSITY
1800
600
RAMAN SHIFT (Δν, cm⁻¹)
(a)
(b)
(c)
1610
1553
1369
1267
1207
1094
1023
934
865
793
550
RAYLEIGH LINE

Table 5 SERS Results for Uridine and 6-Amino Uracil.[a]

Band positions/cm^{-1} (b)			
$\Delta\nu_{Ag}$(uracil)	$\Delta\nu_{Ag}$(uridine)	$\Delta\nu_{Ag}$(6-amino uracil)	Assignment
578 (.20)	550 (.16)	568 (.12)	$N_1C_2N_3{}^B$ - $C_2N_3C_4{}^B$
796 (1.0)	793 (1.0)	684 (1.0)	Ring breathing
	865 (.27)		C-O^S ribose[c]
		972 (.06)	C_6 - N^S
	934 (.16)		C-O^S ribose[c]
1040 (.13)	1023 (.25)	1040 (.11)	Stretching motion of the ring's C-N bonds
1094 (.11)	1094 (.14)		
1207 (.40)	1207 (.20Sh)		-C_6H^B + $C_2N_3{}^S$
1267 (.49)	1267 (.64)	1260 (.08)	Ring^S + CH^B
1381 (.50)	1369 (.61)	1389 (.08)	N_3H^B - C_4 = O^S
1511 (.23)		1485 (.07)	NH^B
1559 (.07Sh)	1553 (.11)	1550 (.13)	
1610 (.30)	1610 (.43)		C_4 = O^S + $C_5C_6{}^S$

(a) Abbreviations as in Table 4.

(b) Values in parentheses are relative intensities.

(c) From reference 49.

bands appear at 865 cm^{-1} and 934 cm^{-1}, which have been attributed to C-O stretching mode in the ribose residue. All the other bands agree well with the already assigned uracil bands. An interesting observation is that the ring breathing vibration at ~793 cm^{-1} is two times smaller than its counterpart in uracil at ~796 cm^{-1}. In uridine, the methoxy group could hydrogen-bond with the oxygen at C_2 restricting the pyrimidine breathing. On the other hand, the intensity of the bands corresponding to C_4=O stretching, at 1610 and 1369 cm^{-1}, does not decrease by the presence of the sugar residue. This may mean that the molecule is actually coordinated to the metal through C_4=O group as suggested previously.

The results obtained for 6-amino uracil are shown in Figure 17 and Table 5. The ring breathing mode has shifted to a lower frequency from 793 to 684 cm^{-1}. Only one new band appears at 972 cm^{-1} which could be assigned to either the C_6-N stretching vibration or the N-H bending vibration but for a definite assignment, a deuterated derivative has to be studied. The bond associated with the C_6H bending vibration (at ~1207 cm^{-1}) in uracil and uridine disappear in the 6-amino uracil spectrum. This is as expected since the amino group is now replacing the hydrogen. The other bands that disappear are those assigned to the C_4=O (at 1610 cm^{-1}) and C_6C_5 (at 1582 cm^{-1}) stretching vibrations. There is a possibility that the molecule is no longer bound to the surface through the C=O group but instead through the amino group at C_6. Other vibrations of the $-NH_2$ group itself do not show because they occur at frequencies higher than the ones shown

Figure 17 Scattered intensity (1 cm = 130 cts/s) vs. Raman shift ($\Delta\nu$, cm^{-1}) of (a) 500 μg/mL 6-amino uracil in water; (b) the silver hydrosols; and (c) 50 μg/mL 6-amino uracil in silver hydrosols (SERS spectrum). The insert figure corresponds to the 684 cm^{-1} surface enhanced band of 5 μg/mL 6-amino uracil.

RELATIVE SIGNAL INTENSITY
RAMAN SHIFT (Δν, cm⁻¹)
1800
600
(a)
(b)
(c)
RAYLEIGH LINE
684
568
1040
972
1550
1485
1389
1260
NH2
N
H
HN
NH
O
O

in the spectrum ($\Delta\nu$ > 2000 cm^{-1}, e.g., at ~3000 cm^{-1} one finds the antisymmetric and symmetric NH stretching vibration; at 1600 cm^{-1} one can find the NH_2 bending (scissors) vibration but this one is a weak band (50)).

The high quality SERS spectra shown in section (c) of Figures 15, 16 and 17 in the presence of the silver hydrosols greatly exceeds that obtained from a solution in the absence of the colloidal particles (compare sections (a) and (c) of Figures 11-13). As will be discussed in the next section, good S/N ratios were obtained in all cases. In section (b) of these figures appears the continuous inelastic scattering of the silver hydrosols before the analyte was added; the only noticeable feature of these scans is a broad band at around 1600 cm^{-1} which is assigned to the -OH bending vibration of the water molecules.

Four other molecules were studied by SERS in order to further demonstrate the usefulness of the technique. These were p-aminobenzoic acid (PABA), phenytoin, 2-aminofluorene and 2-aminonaphthalene; in Figure 18 their molecular structures are shown. The first of these, PABA, is a drug used extensively in pharmaceutical and nutritional products. Its SERS spectrum is shown in Figure 19. The most prominent bands appear at 1582 and 1495 cm^{-1} corresponding to C-C stretching vibrations of benzene ring and at 1359 cm^{-1} corresponding to a stretching vibration of the COO^- group. Following in intensity are a band at 1167 cm^{-1} which could be assigned to C-H in plane bending and a band at 1127 cm^{-1} probably due to NH_2 bending. The bands that appear at frequencies lower than 1000 cm^{-1} are assignable

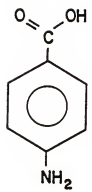

PABA

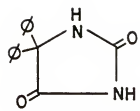

Phenytoin

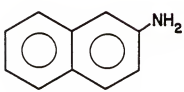

2-aminonapthalene

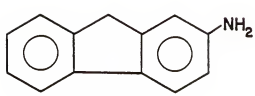

2-aminofluorene

Figure 18 Molecular structures of other adsorbates studied.

Figure 19 Scattered intensity vs. Raman shift of (a) the silver hydrosols (3 cm = 390 cts/s); (b) 80 µg/mL PABA in water (1 cm = 390 cts/s); and (c) SERS spectrum of 50 µg/mL PABA in silver hydrosols (1 cm = 390 cts/s).

RELATIVE SIGNAL INTENSITY
RAMAN SHIFT (Δν, cm⁻¹)
1800
600
(a)
(b)
(c)
RAYLEIGH LINE
1667
1582
1495
1359
1231
1167
1127
979
852
793
O=C-OH
NH2

to benzene ring modes. The absence of a Raman mode in the 1700 cm^{-1} region corresponding to vibration of the COO-H group together with the appearance of a strong band at 1359 cm^{-1} which above was assigned to a stretching vibration of the COO^- group suggests that the molecule is adsorbed in its anionic form. The predominant species at the pH used (around 9) is the anion. Suh et al. (51) have argued that considering the aminobenzoate anion to be almost planar, it is most likely to be π-bonded to the silver surface in a flat orientation rather than perpendicular to the surface. Binding would occur through the lone pairs on either the carboxylate or amine group. They further suggested that this might explain the dominance of benzene vibrations in the SERS spectrum. For comparison purposes, Figure 19 also contains the NRS spectrum for a dilution of the ethanolic stock solution of PABA in water. The bands at around 872, 1033, 1080, 1260 and 1434 cm^{-1} are all assigned to ethanol vibrational modes.

The next molecule studied was phenytoin. Phenytoin is a drug which is widely prescribed for the treatment of epilepsy (52). Traditional methods for its identification include time consuming screening tests which also give a positive response for molecules such as barbiturates, bemegride and primidone (53). Therefore, the development of a method that will allow a rapid identification of the drug is desirable. The SERS spectrum of phenytoin appears in Figure 20. The frequencies at which the bands appear are included in the spectrum to facilitate future reference. No attempts were made to assign the bands to specific vibrational modes of the molecule but the spectrum correlates well with its published NRS spectrum (54).

Figure 20 Scattered intensity (1 cm = 130 cts/s) vs. Raman shift of (a) the silver hydrosols; (b) 0.75 µg/mL phenytoin in water; and (c) 0.75 µg/mL phenytoin in silver hydrosols (SERS spectrum).

RELATIVE SIGNAL INTENSITY
RAMAN SHIFT (Δν, cm⁻¹)
1800
600
(a)
(b)
(c)
RAYLEIGH LINE
677
793
768
1002
1030
1067
1100
1181
1151
1365
1566
1642
HN
O
N
H
Ø
Ø

The two other molecules studied are polycyclic aromatic hydrocarbons (PAHs). These are molecules formed during incomplete combustion of organic materials. It has been known for many years that certain PAHs possess carcinogenic properties. For this reason, analytical methodology for the identification and quantitation of these compounds has undergone rapid growth and development in the past years. Luminescence techniques are very sensitive for PAH determinations. However, the broad overlapping bands observed in fluorescence and phosphorescence spectra render these techniques unapplicable for structure identification; SERS, being a vibrational technique, consists of narrow bands which give definite insights of molecular structure, i.e., it is a more selective technique.

Figure 21 shows the SERS of naphtnalene and two of its derivatives, 2-naphthol and 2-aminonaphthalene. The stronger bands of these spectra could only be assigned to vibrations of the ethanol molecule. The hydrosols did not change color upon addition of these analytes, i.e., no coagulation occurred; therefore, it can be assumed that no adsorption took place as has been previously reported for benzene in silver colloids (55).

Fluorene and 2-aminofluorene, on the other hand, exhibit very different SERS spectra as shown in Figure 22. The spectrum of 2-aminofluorene is a very intense one which correlates well with its structure. The fluorene spectrum, however, resembles those of naphthalene and its derivatives. The amino group in the fluorene molecule induces adsorption onto the silver surface while it has no

Figure 21 Scattered intensity (1 cm = 130 cts/s) vs. Raman shift of (a) 50 μg/mL naphthalene in silver hydrosols; (b) 50 μg/mL naphthol in silver hydrosols; and (c) 50 μg/mL 2-aminonaphthalene in silver hydrosols.

RELATIVE SIGNAL INTENSITY
1800
RAMAN SHIFT (Δν, cm⁻¹)
600
(a)
(b)
(c)
1588
1434
1260
1080
1033
872
RAYLEIGH LINE

Figure 22 Scattered intensity vs. Raman shift of (a) the silver hydrosols (3 cm = 390 cts/s); (b) 50 µg/mL fluorene in silver hydrosols (3 cm = 390 cts/s); and (c) 10 µg/mL 2-aminofluorene in silver hydrosols (1 cm = 390 cts/s).

RELATIVE SIGNAL INTENSITY
1800
RAMAN SHIFT (Δν, cm⁻¹)
600
RAYLEIGH LINE
532
564
603
635
656
716
765
831
1087
1141
1207
1293
1375
1395
1456, 1450
1594
NH2

effect on the adsorption of naphthalene. This can be explained by the greater delocalization of the lone-electron pair of the nitrogen atom in the π system of naphthalene, which decreases the possibility of interaction with the silver surface.

Quantitative Study

The dependence of the intensity of the 1005 cm^{-1} SERS band of phenytoin on concentration was studied under different experimental conditions. In none of the experiments performed was a good correlation between signal intensity and analyte concentration found for phenytoin. Nevertheless, this study was valuable as it determined the optimum conditions for further experimentation. It was found that higher signals are obtained if the hydrosols are aged for just two hours prior to their mixing with the analytes. As discussed earlier, the longer the aging period of the hydrosols, the higher the concentration of analyte needed to induce aggregation in a given period of time. This is because the stabilizing ions on the surface of the particles are less easily displaced. In the same way, for a constant analyte concentration, the time needed to elapse after analyte addition in order to obtain a given signal intensity increases as the aging period of the hydrosol increases (since the signal intensity depends on the extent of the aggregation induced by the analyte addition on the colloidal particles). So, for a phenytoin concentration of 80 $\mu g/mL$ in the sols, a comparable signal intensity was obtained in

(i) 10 minutes after mixing with the sols if they were aged for 24 hours,

(ii) 40 minutes after mixing with the sols if they were aged for 48 hours, and

(iii) no aggregation was induced at this analyte concentration if the sols were aged for 4 days.

If the same experiment is repeated for hydrosols aged for just two hours, a comparable signal intensity as for the above cases is obtained in just 30 minutes for a phenytoin concentration of only 0.75 μg/mL in the sols.

The color of the colloidal dispersions prior to analyte addition also plays an important role in the intensity of the SERS bands of the analytes. As it is widely known, the color of the colloidal solution is an indication of the size of the dispersed particles. A more clear tone of yellow is indicative of smaller paticles in solution, while a brownish-yellow indicates bigger particles and an even darker color of the sols is accompany by turbidity of the solution. An experiment was performed with three colloidal solutions, each differing from the other in the initial color of the colloidal suspension. Again, for a phenytoin concentration of 80 μg/mL, it was found that

(i) for the initially clear yellow suspension, a S/N = 60 is obtained in two hours after adding the analyte to the colloidal solution;

(ii) for the initial brownish-yellow suspension, a S/N = 60 is obtained in 10 minutes after adding the analyte to the colloidal solution; and

(iii) for the initially turbid suspension, precipitation of the colloid was induced by the analyte addition and no SERS was observed.

These results are explained again, on the basis that certain degree of aggregation is needed in order to observe the surface enhanced effect on colloidal suspensions. For the clear yellow sols, initially containing smaller particles in solution, more time is needed to elapse after analyte addition in order for the particles to form the linear strings of aggregates. The growth process will bring the particles into resonance with the laser line, which will excite their surface plasmon polaritrons, a condition that is essential for the observation of the SERS effect. On the other hand, precipitation of the silver will occur in the initially turbid colloidal suspension, suppressing the SERS effect.

The main problem in the quantitation study of phenytoin arose from the interaction that this particular adsorbate has with the silver hydrosols. For low concentrations of adsorbate (<0.75 μg/mL) the SERS effect was not observed presumably because the concentration was too low to induce chain formation. In the concentration range between 0.75 μg/mL and 1.25 μg/mL, aggregation was induced by this adsorbate, and a good correlation between signal intensity and analyte concentration was found. Higher concentrations of analyte, however, caused further coagulation of the colloids leading to the precipitation of metallic silver as could be inferred by the observation of visible particles. This was accompanied by a decrease in the signal while the supernatant solution completely clarified.

Two solutions to this problem were postulated. First, it is an experimental fact that, at least under some circumstances, an adsorbed polymer stabilizes a dispersion against flocculation. In fact, organic molecules with large nonpolar groups are known to adsorb strongly to the surface of metal colloids allowing in this way the observation of their SERS spectra (56-59). Thus, a series of experiments were performed in which three different stabilizers, namely, polyvinyl alcohol (PVA) at 0.1% v/v concentration, sodium dodecylsulfate (SDS) at $5X10^{-2}$ M concentration and cetylpyridium chloride at $1.2X10^{-3}$ M concentration were used as protective agents. These were added to the colloidal suspensions up to the above mentioned concentrations either before or after analyte addition. In neither case could the analyte displace the stabilizers from the colloidal surface, and thus no SERS spectrum could be observed from it.

The second approach was to change the initial concentration of the reagents used to prepare the colloidal suspension so as to change the final number of available silver sites in solution. Lower concentrations of reagents are expected to produce a smaller number of larger particles in solution, while more concentrated reagents should produce larger number of smaller particles. As a first inference, it seems rather logical to suppose that a diluted silver hydrosol would require less analyte to bring about aggregation than a concentrated one since there is a smaller number of particles to be acted upon by the analyte. There are, however, other factors to be considered. Upon dilution of the hydrosol, the suspended particles become more

widely separated and, as a result, the probability of collision is decreased. The predominance of one or the other of these processes defines the effect of the concentration of the sols. It can be inferred from Table 6 that better signals are obtained at intermediate concentrations of hydrosols where these effects can be regarded as nearly equal. At the lower concentration extreme, lower signals are obtained reflecting the predominance of the dilution effect. Similarly, this effect also dominates at higher concentrations, and even though there are more silver sites available for analyte adsorption the particles are closer together and the addition of the analyte brings about complete coagulation and thus a decrease in the SERS intensity.

A quantitative study was also performed on the other adsorbates reported in the previous section. Uracil and its derivatives behaved similarly as already described for phenytoin and at concentrations as low as 5 μg/mL complete coagulation of the hydrosols was observed. Surprisingly, however, good calibration curves were obtained for PABA and 2-aminofluorene. In Figure 23, the logarithmic calibration plots of these compounds are shown. The data were obtained with the 1359 cm^{-1} and 1594 cm^{-1} Raman bands of PABA and 2-aminofluorene, respectively. For both cases, the curves are linear for almost two orders of magnitude. From the linear calibration plots and the noise measurements, it is estimated, as shown in Table 7, that for both analytes the detection limits are in the sub μg/mL range. Considering that the laser beam was only illuminating a 0.071 cm^3 cuvette

Table 6 Effect of the Concentration of Silver Hydrosol on the SERS Signal of 0.75 µg/mL Phenytoin.

Concentration of silver sols (M)	SERS relative signal intensity
$2.5X10^{-5}$	1.3
$1.5X10^{-4}$	15
$2.5X10^{-4}$	13
$5X10^{-4}$	3.0

Figure 23 Logarithmic calibration plot for PABA at the 1359 cm^{-1} Raman band and for 2-aminofluorene at the 1594 cm^{-1} Raman band.

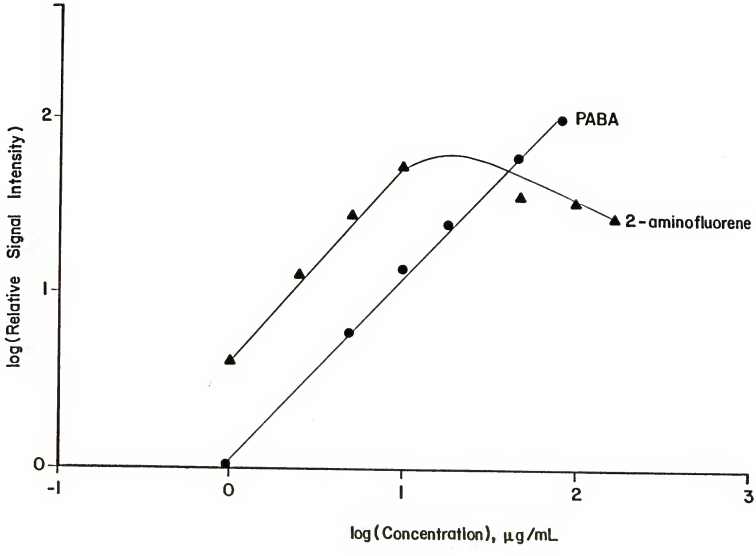
log (Relative Signal Intensity)
2
1
0
-1
0
1
2
3
log (Concentration), µg/mL
PABA
2-aminofluorene

Table 7 SERS Limits of Detection[a] and Calibration Sensitivities for PABA and 2-Aminofluorene.

	PABA	2-Aminofluorene
Calibration sensitivities (RSI[b] /μg/mL)	1.21	5.44
C_L (μg/mL)	0.5	0.1
Correlation coefficient	.997	.993
Slope of log-log calibration curve	1.05	1.13

(a) $C_L = 3\ S_B/M$, where C_L is the limit of detection in μg/mL, S_B = 1/5 peak to peak noise and m is the slope of the linear calibration curve (i.e., the calibration sensitivity).

(b) Relative Signal Intensity.

volume, the optical limits of detection are 35 ng and 7 ng for PABA and 2-aminofluorene, respectively. It should be mentioned at this point that better limits of detection should be obtained by tuning the laser to the peak absorption maximum of the surface plasmon polaritrons, at which point the maximum surface enhancement effect would be obtained.

The maximum signal obtained as the concentration of analyte was increased reflects saturation of available interaction sites at the silver surface as has been pointed out by others (32,38). This is accompanied by the precipitation of metallic silver as discussed earlier. The concentration at which the maximum signal is reached is characteristic of the particular analyte under study. Working curves for concentrations under this limiting value should have a linear response. The intensity of the Raman band under study will slowly decrease towards the unenhanced value as the concentration is increased.

Finally, since the NRS spectrum could not be measured with the spectrometer used, no enhancement factors could be calculated for the SERS observed. However, for the most intense bands of all the molecules studied, a depolarization ratio (p) greater than 0.7 could be deduced from the depolarization study, which is typical for SERS bands.

CHAPTER FIVE
CONCLUSIONS AND FUTURE WORK

The experimental results clearly demonstrate that an analytical method based on SERS provides high spectral selectivity and identification power as well as analytical sensitivity and detection power for the study of N-containing drugs and PAHs. The experimental arrangement used throughout this work possesses several advantages: simplicity, lower cost, better S/N ratios, faster scan rates and no time consuming precise optical adjustments of the Raman scattered radiation into the monochromator slit is necessary.

The use of colloidal hydrosols as substrates for SERS provides a number of advantages that include ease of formation and manipulation, continuous renewal of the sample by flow through the light beam, characterization by simple absorption techniques and a simple dependence of the enhancement on particle size and shape. Furthermore, the large Raman band enhancements of species adsorbed at the surface of silver colloids permit not only quantitative and qualitative studies, but also structural and kinetic studies similar to those at roughened electrode surfaces.

Their main disadvantage, however, is the instability of the hydrosols after analyte addition. In some cases this can bring about complete coagulation of the suspension and often renders the results

irreproducible and dependent on factors, such as the way the analyte is added and the stirring processes before and/or after analyte addition. In order to improve this, studies are currently (J.J. Laserna, personal communication) underway on the stability of silver hydrosols as a function of silver nitrate and sodium borohydride relative concentrations, of solution mixing and of solution temperature before and after the reduction. After these parameters are optimized, the approach taken by Tran (31,60) and Séquaris and Koglin (47) of stabilizing the silver colloidal hydrosols with filter paper supports (cellulose, glass or quartz fibers) could be followed. This could lead to a greater applicability of the technique, especially for those analytes (as uracil derivatives) which rapidly flocculate the colloids even at very low adsorbate concentrations. This makes their quantitation almost impossible due to the very limited useful analytical ranges observed.

Overall, the technique is still in its infancy and many figures of merit, including limit of detection, precision, linear dynamic range, selectivity, sensitivity and reproducibility, remain to be reported for the various adsorbates of current analytical interest. For the future, we can foresee that SERS spectroscopy most likely can be applied as a selective detector for high performance liquid chromatography (HPLC). Two proposed designs for such a detector are shown in Figure 20.

In the first suggested design, shown in Figure 24(a), the silver hydrosols are circulated with a peristaltic pump through one of the

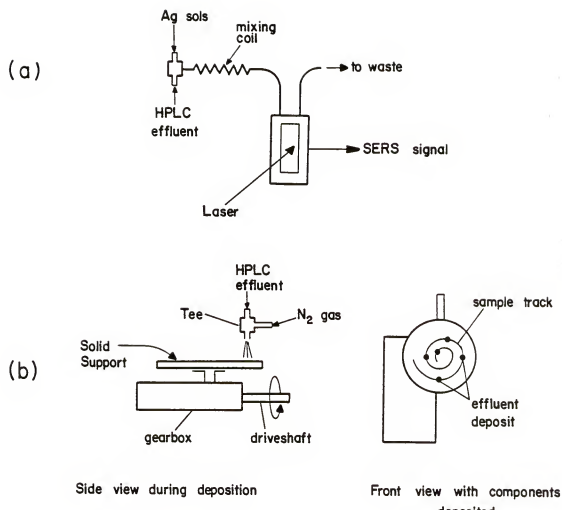

Figure 24 Proposed HPLC detectors: (a) flow-through design; and (b) solid support design.

tee ports of a mixing tee (commercially available with internal volumes as low as 0.62 μL) where it is mixed with the HPLC effluent coming from another tee port. The mixture is then passed through a coil which further mixes the reagents and forms the aggregated colloids to be sent to a rectangular flow-through cell positioned at 90° to the laser beam. This type of arrangement minimizes sample heating by the laser and avoids photodecomposition of the species of interest. The SERS spectrum can be detected by either a photomultiplier, using a stop-flow method, or by an intensified photodiode array detector which allows a continuous analysis of the chromatographic effluent.

The second suggested diagram, Figure 24b, is very similar to one recently proposed by Gagel and Biemann (61) for the continuous recording of Fourier transform infrared spectra of the effluent of a microbore HPLC. The HPLC effluent is again connected to one of the ports of a mixing tee where, in this case, it is mixed with and pressurized by nitrogen gas which is introduced from a short length tubing attached to another tee port. Thus nebulized, the effluent is then directed to a solid support previously treated with silver hydrosols through a syringe tip fitted to the third tee port. The solid support is placed in a gearbox which is rotated slowly by a stepping motor.

After the deposition of the chromatographic effluent, the device could be placed in the sample compartment of a Raman system where it is again rotated in front of a laser beam. The front surface SERS spectrum can be detected by an intensified photodiode array

detector. The design of this device provides the advantage that the spectral data could be ennanced by signal averaging several scans. Another advantage of the design is that during the collection step, the motor speed could be reduced to enhance sensitivity by concentrating more material in a smaller area. This system may prove to be particularly useful for samples that are dissolved into water immiscible solvents or for normal phase HPLC where the immiscibility of the solvents with the hydrosols may be a problem when using the first proposed system.

REFERENCES

1. M. Fleischmann, P.J. Hendra and A.J. McQuillan, Chem. Phys. Lett., 26, 163 (1974).

2. D.L. Jeanmarie and R.P. van Duyne, J. Electroanal. Chem., 84, 1 (1977).

3. M.G. Albrecht and J.A. Creighton, J. Am. Chem. Soc., 99, 5215 (1977).

4. R.K. Chang and T.E. Furtak (Eds.), Surface Enhanced Raman Scattering, Plenum Press, New York, 1982.

5. T.E. Furtak and J. Reyes, Surf. Sci., 93, 351 (1980).

6. A. Otto, Appl. Surf. Sci., 6, 309 (1980).

7. H. Seki, J. Electron Spectros. Rel. Phenom., 39, 289 (1986).

8. J.I. Gersten and A. Nitzan, in Surface Enhanced Raman Scattering, ed. by R.K. Chang and T.E. Furtak, Plenum Press, New York, 1982.

9. T.E. Furtak, J. Electroanal. Chem., 150, 375 (1983).

10. J. Billman, G. Kovacs and A. Otto, Surf. Sci., 92, 153 (1980).

11. E. Burstein, Y.J. Chen, C.Y. Chen, S. Lundquist and E. Tossatti, Solid State Commun., 29, 567 (1979).

12. H.A. Laitinen and W.E. Harris, Chemical Analysis, 2nd Ed., McGraw-Hill Series in Advanced Chemistry, New York, 1975.

13. D.J. Shaw, Introduction to Colloid and Surface Chemistry, 2nd Ed., Butterworths, London, 1970.

14. P.C. Hiemenz, Principles of Colloid and Surface Chemistry, 2nd Ed., Marcel Dekker, Inc., New York, 1986.

15. R.P. van Duyne, in Chemical and Biochemical Applications of Lasers, Vol. 4, ed. by C.B. Moore, Academic Press, New York, 1979.

16. J.A. Creighton, C.G. Blatchford and M.G. Albrecht, J. Chem. Soc. Faraday II, 75, 790 (1979).

17. J.A. Creighton, in Surface Enhanced Raman Scattering, ed. by R.K. Chang and T.E. Furtak, Plenum Press, New York, 1982.

18. M. Kerker, D.-S. Wang and H. Chew, Appl. Opt., 19, 4159 (1980).

19. J.I. Gersten, J. Chem. Phys., 72, 5779 (1980).

20. D.-S. Wang and M. Kerker, Phys. Rev. B, 24, 1777 (1981).

21. C.G. Blatchford, J.R. Campbell and J.A. Creighton, Surf. Sci., 120, 435 (1982).

22. C.G. Blatchford and J.A. Creighton, in Vibrations at Surfaces, ed. by R. Caudano, J.-M. Guilles and A.A. Lucas, Plenum Press, New York, 1982.

23. J.A. Creighton, in Surface Studies with Lasers, ed. by F.R. Aussenegg, A. Leitner and M.E. Lippitsch, Springer-Verlag, New York, 1983.

24. M. Kerker, D.-S. Wang, H. Chew, O. Siiman and L.A. Bumm, in Surface Enhanced Raman Scattering, ed. by R.K. Chang and T.E. Furtak, Plenum Press, New York, 1982.

25. D.A. Uleitz, S. Garoff and T.J. Gramila, Opt. Lett., 7, 168 (1982).

26. J.D. Winefordner, S.G. Schulman and T.C. O'Haver, Luminescence Spectrometry in Analytical Chemistry, Wiley-Interscience, New York, 1972.

27. L. de Galan, Analytical Spectrometry, Adam Hilger Ltd., London, 1971.

28. W. Demtröder, Laser Spectroscopy, 2nd Ed., Springer-Verlag, New York, 1982.

29. M.S. Epstein and J.D. Winefordner, Prog. Anal. Atom. Spectrosc., 7, 67 (1984).

30. J.E. Pemberton and R.P. Buck, Anal. Chem., 53, 2263 (1981).

31. C.D. Tran, Anal. Chem., 56, 824 (1984).

32. T. Vo-Dinh, M.Y.K. Hiromoto, G.M. Begun and R.L. Moody, Anal. Chem., 56, 1667 (1984).

33. T. Vo-Dinh, M. Meier and A. Wokaun, Anal. Chim. Acta, in press.

34. M. Meier, A. Wokaun and T. Vo-Dinh, J. Phys. Chem., 89, 1843 (1985).

35. P.U. Enlow, M. Buncick, R.J. Warmack and T. Vo-Dinh, Anal. Chem., 58, 1119 (1986).

36. C. Jennings, R. Aroca, A.-M. Hor and R.O. Loutfy, Anal. Chem., 56, 2033 (1984).

37. E. Gautner, D. Steinert and J. Reinhardt, Anal. Chem., 57, 1658 (1985).

38. R.-S. Sheng, L. Zhu and M.D. Morris, Anal. Chem., 58, 1116 (1986).

39. P.C. Lee and D. Meisel, J. Phys. Chem., 86, 3391 (1982).

40. M. Kerker, O. Siiman, L.A. Bumm and D.-S. Wang, Appl. Opt., 19, 3253 (1980).

41. E. Koglin, J.M. Séquaris and P. Valenta, J. Mol. Struct., 60, 421 (1980).

42. K.M. Ervin, E. Koglin, J.M. Séquaris, P. Valenta and H.W. Nürmberg, J. Electroanal. Chem., 114, 179 (1980).

43. E. Koglin, J.M. Séquaris and P. Valenta, J. Mol. Struct., 79, 185 (1982).

44. C. Otto, T.J.J. van den Tweel, F.F.M. de Mul and J. Greve, J. Raman Spectrosc., 17, 289 (1986).

45. E. Koglin, J.M. Séquaris and P. Valenta, in Surface Studies with Lasers, ed. by F.R. Aussenegg, A. Leitner and M.E. Lippitsch, Springer-Verlag, New York, 1983.

46. E. Koglin, J.M. Séquaris, J.C. Fritz and P. Valenta, J. Mol. Struct., 114, 219 (1984).

47. J.M. Séquaris and E. Koglin, Fresenius Z. Anal. Chem., 321, 758 (1985).

48. M. Tsuboi, S. Takahashi and I. Harada, Physicochemical Properties of Nucleic Acids, ed. by J. Duchesne, Academic Press, New York, 1973.

49. R.C. Lord and G.J. Thomas, Jr., Spectrochim. Acta, 23A, 2551 (1967)

50. F.R. Dollish, W.G. Fateley and F.F. Bentley, Characteristic Frequencies of Organic Compounds, Wiley-Interscience, New York, 1974.

51. J.S. Sun, D.P. Di Lella and M. Moskovits, J. Phys. Chem., 87, 1540 (1983).

52. J.S. O'Neal, K.B. Sloan and S.G. Schulman, J. Pharm. Biomed. Anal., 4, 103 (1986).

53. E.G.C. Clarke, Isolation and Identification of Drugs, The Pharmaceutical Press, London, 1969.

54. The Sadler Standard Spectra, Raman Number 2583, Sadler Research Laboratories, Philadelphia, PA.

55. M.E. Lippitsch, Chem. Phys. Lett., 74, 125 (1980).

56. P.C. Lee and D. Meisel, Chem. Phys. Lett., 99, 262 (1983).

57. U. Siiman, L.A. Bumm, R. Callaghan, C.G. Blatchford and M. Kerker, J. Phys. Chem., 87, 1014 (1983).

58. S.M. Heard, F. Grieser and C.G. Barraclough, Chem. Phys. Lett., 95, 154 (1983).

59. S.M. Heard, F. Grieser and C.G. Barraclough, J. Phys. Che., 89, 389 (1985).

60. C.D. Tran, J. Chromatogr., 292, 432 (1984).

61. J.J. Gagel and K. Biemann, Anal. Chem., 58, 2184 (1986).

BIOGRAPHICAL SKETCH

Lisie was born on October 28, 1959, in San Juan, Puerto Rico. Her parents are Edilberto Torres Ríos and Ana Lydia Tapia de Torres. She attended Colegio Santa Rosa in Bayamón, Puerto Rico, where she received her high school diploma in 1977.

She graduated from the University of Puerto Rico, Mayagüez, in 1981, receiving a Bachelor of Science degree in chemistry. Since then, she has attended the University of Florida where she received her Master of Science degree in analytical chemistry in 1983 and her Ph.D. degree in analytical chemistry in 1986, both under the supervision of Dr. James D. Winefordner.

I certify that I have read this study and that in my opinion it conforms to acceptable standards of scholarly presentation and is fully adequate, in scope and quality, as a dissertation for the degree of Doctor of Philosophy.

James D. Winefordner, Chairman
Graduate Research Professor of Chemistry

I certify that I have read this study and that in my opinion it conforms to acceptable standards of scholarly presentation and is fully adequate, in scope and quality, as a dissertation for the degree of Doctor of Philosophy.

John G. Dorsey
Associate Professor of Chemistry

I certify that I have read this study and that in my opinion it conforms to acceptable standards of scholarly presentation and is fully adequate, in scope and quality, as a dissertation for the degree of Doctor of Philosophy.

Anna Brajter-Toth
Assistant Professor of Chemistry

I certify that I have read this study and that in my opinion it conforms to acceptable standards of scholarly presentation and is fully adequate, in scope and quality, as a dissertation for the degree of Doctor of Philosophy.

Samuel Colgate
Associate Professor of Chemistry

I certify that I have read this study and that in my opinion it conforms to acceptable standards of scholarly presentation and is fully adequate, in scope and quality, as a dissertation for the degree of Doctor of Philosophy.

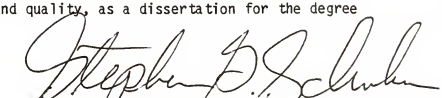

Stephen G. Schulman
Professor of Pharmacy

This dissertation was submitted to the Graduate Faculty of the Department of Chemistry in the College of Liberal Arts and Sciences and to the Graduate School and was accepted as partial fulfillment of the requirements for the degree of Doctor of Philosophy.

December, 1986

Dean, Graduate School